ADVANCING EARTH AND SPACE SCIENCE

Tectonics

RESEARCH ARTICLE

10.1029/2021TC006882

Key Points:

- Anisotropy of magnetic susceptibility data from Neogene rocks in SW Anatolia yield orientations of principal tectonic strain
- SW Anatolia underwent E-W, and then NW-SE oriented extension in the Oligocene to middle Miocene and late Miocene to Pliocene, respectively
- Deformation is the result of SW directed stretching of the over-riding lithosphere above the southward retreating subducted African oceanic slab

Correspondence to:

N. Kaymakcı,
kaymakci@metu.edu.tr

Citation:

Özkaptan, M., Gülyüz, E., Uzel, B., Langereis, C. G., Özacar, A. A., & Kaymakcı, N. (2021). Deformation in SW Anatolia (Turkey) documented by anisotropy of magnetic susceptibility data. *Tectonics*, *40*, e2021TC006882. https://doi.org/10.1029/2021TC006882

Received 28 APR 2021
Accepted 23 NOV 2021

Author Contributions:

Conceptualization: Erhan Gülyüz, Bora Uzel, Cor G. Langereis, A. Arda Özacar, Nuretdin Kaymakcı
Formal analysis: Murat Özkaptan, Erhan Gülyüz, Cor G. Langereis, Nuretdin Kaymakcı
Funding acquisition: Cor G. Langereis, Nuretdin Kaymakcı
Investigation: Murat Özkaptan, Erhan Gülyüz, Cor G. Langereis, Nuretdin Kaymakcı
Methodology: Murat Özkaptan, Bora Uzel, Cor G. Langereis, A. Arda Özacar, Nuretdin Kaymakcı
Project Administration: Bora Uzel, Cor G. Langereis, A. Arda Özacar, Nuretdin Kaymakcı
Software: Murat Özkaptan
Supervision: Cor G. Langereis, Nuretdin Kaymakcı
Validation: Murat Özkaptan, Cor G. Langereis, Nuretdin Kaymakcı

Deformation in SW Anatolia (Turkey) Documented by Anisotropy of Magnetic Susceptibility Data

Murat Özkaptan[1], Erhan Gülyüz[2,3], Bora Uzel[4], Cor G. Langereis[5], A. Arda Özacar[6], and Nuretdin Kaymakcı[6]

[1]Department of Geophysical Engineering, Karadeniz Technical University, Trabzon, Turkey, [2]Department of Geological Engineering, Van Yüzüncü Yıl University, Van, Turkey, [3]Now at Department of Neotectonics and Thermochronology, Institute of Rock Structure and Mechanics of the Czech Academy of Science, Prague, Czech Republic, [4]Department of Geological Engineering, Dokuz Eylül University, İzmir, Turkey, [5]Department of Earth Sciences, Paleomagnetic Laboratory Fort Hoofddijk, Utrecht University, Utrecht, The Netherlands, [6]Department of Geological Engineering, Middle East Technical University, Ankara, Turkey

Abstract Convergence between the Eurasian and the African plates in the West Anatolian-Aegean region results in a trench retreat due to slab roll-back and tearing of the subducted African lithosphere. The upper plate response of this process gave way to back-arc extension in the region. We have conducted a very detailed anisotropy of magnetic susceptibility (AMS) study on the Neogene rocks in SW Anatolia to unravel the style and magnitudes of deformation. For this purpose, from 83 sites in 11 structurally homogeneous domains, 1,680 paleomagnetic samples were analyzed. The results show that AMS fabrics are related to the tectonic deformation and that the magnetic lineation (maximum susceptibility axis, k_1) is parallel to inferred maximum extension, while minimum susceptibility (k_3) is typically normal to the bedding plane, corresponding to a preserved compaction associated with deposition fabric. The intermediate axis (k_2) is parallel to a second extension direction and indicates that the region has been under the control of multi-directional extension during the Neogene. Two main magnetic lineation directions are identified and represent Oligocene to middle Miocene E-W, and late Miocene to Pliocene NW-SE oriented extension. The magnetic lineation directions are dominantly parallel or perpendicular to the general strikes of the normal faults. The results show that the deformation in the region resembles two differentially stretched rubber sheets under the influence of SW oriented extension, exerted by the southward retreating Eastern Mediterranean subduction system.

Plain Language Summary The tectonic style and amount of crustal deformation in SW-Anatolia are revealed by sets of anisotropy of magnetic susceptibility data obtained from SW Anatolia. The orientation of principal strain axes changes gradually although the shape of the strain ellipsoid among all the rocks in late Miocene to Pliocene domains remains the same. Based on these results and published information, we conclude that the SW Anatolia is under the control of multi-directional extension associated with counterclockwise rotation exerted by the southward retreat of the Eastern Mediterranean subduction system (Hellenic-Pliny-Strabo and Cyprian Trenches). The retreat resulted in stretching of SW Anatolia, the over-riding plate, to accommodate the retreat of the trench as a non-rigid, stretched rubber-sheet like deformation style, which seems to be pulled from a single point toward the SW. The Büyük Menderes-Denizli-Baklan grabens and Dinar-Aksu faults mark the northern boundary of this peculiar and active deformation zone.

1. Introduction

The anisotropy of magnetic susceptibility (AMS) in weakly deformed rocks can be used to provide information on the sedimentary and tectonic history of rocks because there is typically a relationship between the AMS tensor (ellipsoid) and the stress and resulting strain field of the area. The shape of the AMS ellipsoid in sedimentary rocks depends on the shape and distribution of magnetic grains in a rock volume (the magnetic fabric), and it is closely related to deformation; hence to the strain ellipsoids (Lüneburg et al., 1999; Oliva-Urcia et al., 2010; Rochette et al., 1992). The magnetic fabric is controlled by primary geologic processes, such as compaction and current flow that produce purely sedimentary magnetic fabrics. However, secondary factors, such as related to tectonic deformation are also important factors in the development of the magnetic fabric, and they often replace the primary sedimentary fabric. Authigenic minerals and fine-grained clastic deposits, such as clays, which accumulate by vertical deposition in a low-energy environment, often lack visible primary sedimentary structures

Writing – original draft: Murat Özkaptan, Cor G. Langereis, Nuretdin Kaymakcı
Writing – review & editing: Murat Özkaptan, Cor G. Langereis, Nuretdin Kaymakcı

and paleocurrent features. Therefore, they also lack an interpretable primary depositional environment fabric. Discrimination between the primary and secondary (post-depositional) features is very crucial in the utilization of AMS ellipsoid as a strain marker. Nevertheless, sediments may lack directional markers but the compactional fabric is well developed with k_3 perpendicular to beddings plane and $k1$ and $k2$ dispersed in the foliation plan.

Classic methods for the determination of strain ellipsoids for sedimentary rocks involves clast-based measurements such as clast geometry, orientations, texture, and packing (Ramsey & Huber, 1983). However, AMS-based strain determination techniques in low to weakly deformed sedimentary rocks have the potential to quantify principal strain axes using the character and distribution of magnetic grains in rock volumes (Borradaile & Henry, 1997; Hirt et al., 1993; Lüneburg et al., 1999; Oliva-Urcia et al., 2010; Parés & van der Pluijm, 2002; Rochette et al., 1992; Sagnotti & Speranza, 1993).

Deformation related to tectonic processes is often recorded in sedimentary basin sequences. Deciphering the tectonic deformation recorded in sedimentary basins provides information on the basic geologic/tectonic processes that have acted upon the rock, although qualitative and quantitatively definition of these processes is not always possible using classical geologic tools such as grain-based techniques, especially in the absence of penetrative deformation. Although paleostress analyses conducted directly on fault surfaces provide clues about the strain axes, they are always discrete and result from inhomogeneous deformation, which does not always reflect the regional strain ellipsoid. The AMS technique, on the other hand, is an alternative and effective method for the determination of a strain ellipsoid in low to weakly deformed sedimentary rocks (e.g., Scheepers & Langereis, 1994). Care must be given to the fact that the minimum strain axis (k_3) almost always corresponds to primary sedimentary compaction (Duermeijer et al., 1998; Tarling & Hrouda, 1993).

This work collected abundant AMS data that we use to quantify and unravel deformation styles in the late Oligocene-Neogene basins in SW Anatolia, where extensional deformation involving vertical axis rotations took place (Kaymakcı et al., 2018) related to slab edge processes at the over-riding plate of the Aegean-Cyprian subduction system. These include the Acıpayam, Burdur, Çameli, Denizli, Elmalı, Ören and Tavas basins (Figure 1), which are characterized by continental deposits. The basins (a) spatially cover almost all of SW Anatolia where the Menderes Core Complex, Lycian Nappes, and Tauride Platform rocks are exposed and (b) temporally cover the Oligocene to Pliocene time interval, which includes the exhumation of the Menderes Core Complex, the emplacement of the Lycian Nappes and the subduction history of the African oceanic lithosphere along the eastern Mediterranean trenches (Figure 1; Alçiçek, 2007; Alçiçek et al., 2013; Biryol et al., 2011; Hayward, 1984; Le Pichon & Angelier, 1979; van Hinsbergen, Dekkers et al., 2010; van Hinsbergen, Kaymakcı, et al., 2010).

Except for the senses and magnitudes of Neogene rotations in the region (e.g., Kaymakcı et al., 2018; van Hinsbergen, Dekkers et al., 2010; van Hinsbergen, Kaymakcı, et al., 2010), the studies concerned with the quantification of deformation amounts and the strain related to the ongoing tectonic processes in the region are relatively rare. Few studies are focused on the temporal and tectonostratigraphic records of these geologic processes, and these concentrate on only a few basins in the region or are based on regional stratigraphic correlations (Alçiçek et al., 2019; Kaymakcı, 2006; Özkaptan et al., 2018 and references therein).

Seismic tomography studies have shown that the subducted African oceanic slab is fragmented in the mantle (Biryol et al., 2011; Faccenna et al., 2006; van Hinsbergen, Dekkers et al., 2010; van Hinsbergen, Kaymakcı, et al., 2010) and gave way to differential stretching on the overriding plate, SW Anatolia and the Aegean region (Figure 1). Related to this process, one of the ongoing debates concerns the surface expressions of the fragmented African slab in SW Anatolia. It is generally accepted that the fragmented subducted slab below SW Anatolia produced a tear that provided a mantle window below western Anatolia (Biryol et al., 2011; Faccenna et al., 2006; Govers & Wortel, 2005; Kaymakcı et al., 2018; Wortel & Spakman, 2000). Some studies argued that this tear is coupled with the overriding plate and produced a large sinistral strike-slip shear zone in SW Anatolia (e.g., Elitez et al., 2016; Elitez & Yaltırak, 2016; Hall et al., 2014). Others, however, claimed that that the available kinematic data in the region are still insufficient to corroborate the strike-slip mechanism. Some recent studies (e.g., Alçiçek, 2015; Kaymakcı et al., 2018; Özkaptan et al., 2014, 2018) have shown that SW Anatolia is deforming under a very strong extensional setting coupled with a regional counterclockwise rotation. The magnitude and sense of rotation in SW Anatolia increases from east to west and north to south, with no remarkable changes reported in relation to the assumed shear zone. Based on this information, Kaymakcı et al. (2018) argued that the subducted slab and the overriding plate are not coupled to produce a continuous shear zone from the mantle

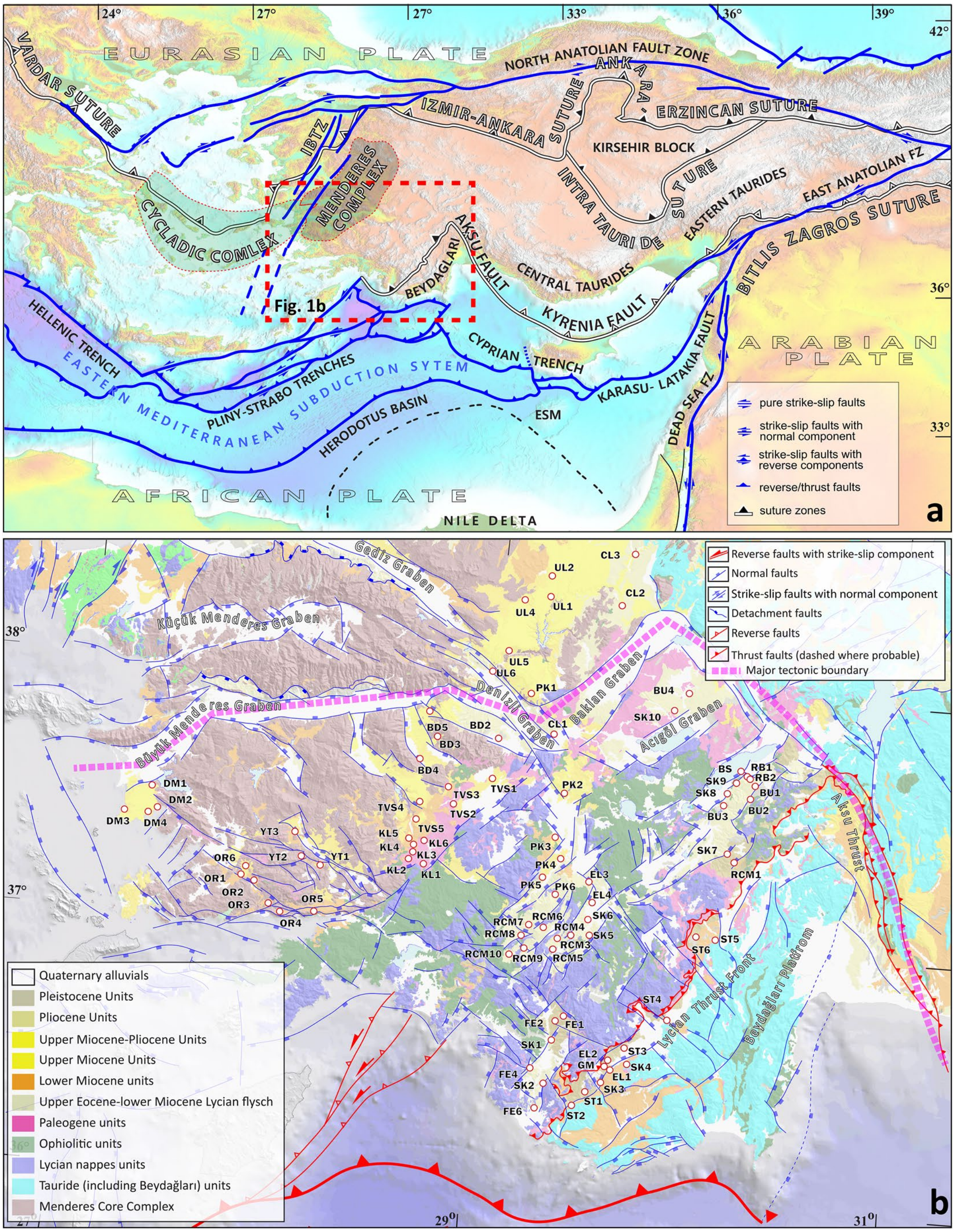

Figure 1. (a) Simplified tectonic scheme of the eastern Mediterranean region. (b) Simplified geologic map of SW Anatolia showing AMS sample locations and major faults (Kaymakcı et al., 2018; General Directorate, MTA, 2002).

up to the surface. Therefore, the slab tear in the northern edge of the subducted part of the African slab does not penetrate the overriding plate, but it is thought to be responsible for the distributed differential extensional strain in the region. The differential retreat of the segmented subducted African Slab in the mantle is expressed in the form of rotational (counterclockwise) and extensional deformation on the SW Anatolian crust (Kaymakcı et al., 2018; Özkaptan et al., 2014).

In this contribution, we investigate the kinematic evolution of SW Anatolia based on newly acquired AMS data collected from the Oligocene-Neogene basins in the region. The data cover Oligocene to Pliocene sedimentary records of SW Anatolian basins, which are constrained temporally by newly established biostratigraphic data of Alçiçek et al. (2019). The main purpose of this study is to quantify the amounts of total cumulative deformation in the region and to establish the orientation of the principal strain axes in the Neogene sequences in the region based on AMS data.

2. Methods

2.1. Sampling

In total, 2,138 standard paleomagnetic samples were drilled in 11 domains consisting of a total of 83 sites in SW Anatolia. Samples were collected from in Eocene-Oligocene (11 sites/519 cores) and Miocene (49 sites/883 cores) marine sediments (limestones, marls, and sandstones) and in Miocene to Pliocene (23 sites/736 cores), lacustrine to continental detrital rocks (mudstones, claystone, and siltstones; Figure 1 and Table 1). In all sampling locations, the weathered surface was removed to reach fresh sedimentary rocks. Care was taken to sample away from active faults and other possible disturbance (e.g., chemical or volcanic) near the sampled sites. The standard cylindrical samples (25 mm Ø) were obtained using a handheld gasoline-powered motor drill or an electric drill with a generator, depending on the rock type in the sites, both equipped with water-cooled diamond-coated drill bits. Both core orientations and bedding attitudes were always measured in the field using a magnetic compass, later corrected for the present-day declination (4.5°W for the entire sampling period, June 2013). Drilled sample cores were marked, wrapped in aluminum foil, and put in protective plastic bags. Because the collected samples were used for many paleomagnetic purposes (determining tectonic vertical axis block-rotations as well as magnetostratigraphy), the number of samples taken per site is variable; a minimum of 13 but—at some localities for magnetostratigraphy—it can reach a maximum of ~400 samples. Ages of the sampled rock types are adopted from Kaymakcı et al. (2018), Konak and Şenel (2002), and Şenel (2002).

2.2. Thermomagnetic Experiments

Before the AMS measurements, at least one thermomagnetic measurement was carried out for each sampled site in order to characterize the magnetic minerals present on samples. Thermomagnetic runs were carried out in air, and the total magnetic moment versus temperature (*M*/*T*) diagrams was obtained using a modified horizontal translation type Curie-balance with a sensitivity of ~5×10^{-9} Am^2 (Mullender et al., 1993). Depending on the intensity of the expected magnetic carrier, about 50–100 g of powdered material from one specimen in each site was put into a quartz glass sample holder and held in place by quartz wool. We used the following heating-cooling cycles (in °C): 20–150, 50–250, 150–350, 250–400, 300–450, 350–525, 420–580, and 500–700 respectively. The maximum temperature level reached is 700°C, finally cooling down to 20°C (room temperature). The successive heating and cooling rates were 10°C/min in air. Based on the results, Curie temperatures were determined following (Fabian et al., 2013) and one representative curve for each of the 11 identified domains is illustrated in Figure 2 and summarized in Table 1.

2.3. AMS Measurements

The collected samples were cut to standard paleomagnetic specimen size with a dual blade rock saw (ASC Scientific, Carlsbad, CA, USA). Because the AMS results are more affected by shape of the specimens than the other paleomagnetic methods, only unbroken, crack-free, and whole specimens are used for AMS measurements. Generally, the cores collected from the field were sufficiently long enough to provide more than one standard specimen. They are divided into subsamples and used for other paleomagnetic purposes. Optimum height/diameter ratio for specimen size varies between 0.8 and 0.9 (Collinson, 1983; Noltimier, 1971; Scriba & Heller, 1978). A total of 1,680 specimens out of more than 2,000 samples collected from the field were analyzed for AMS purposes (Table 1). The AMS was measured with an automatic field variation (low field, 200 A/m) susceptometer using the Multi-Function Kappabridge (MFK1-FA AGICO-Brno, Czech Republic), equipped with an up-down mechanism and a rotator. The measurement sensitivity is 10^{-8} SI, which is very critical for some sedimentary rocks (especially limestones), that exhibit very weak magnetic susceptibility. All measurements and analyses were conducted at the Fort Hoofddijk Paleomagnetic Laboratory of Utrecht University (The Netherlands). Anisoft 4.2 data browser (Chadima & Jelinek, 2009) was used for the display of AMS results and their density distributions

Table 1

Anisotropy of Magnetic Susceptibility Results From Lower Miocene to Pliocene Strata From the SW Anatolia

Locality	Site	Geographic coordinates (°) Latitude (N)	Longitude (E)	N_{AMS}	Age	Rock	Bedding Strike/dip	$k_m \times 10^{-6}$ (SI)	L	F	P_j	T	BTC D/I (k_1)	BTC D/I (k_2)	BTC D/I (k_3)	TC D/I (k_1)	TC D/I (k_2)	TC D/I (k_3)	e_1	e_2	e_3
Acıpayam	~~PK2~~	~~37.5845~~	~~29.3505~~	~~16~~	~~Plio.~~	~~Limestone~~	~~193/18~~	~~0005.7~~	~~1.086~~	~~1.079~~	~~1.181~~	~~0.045~~	~~058.9/42.3~~	~~299.1/28.6~~	~~187.3/34.3~~	~~043.0/53.5~~	~~297.4/11.2~~	~~199.7/34.3~~	~~45.2~~	~~54.5~~	~~50.0~~
	PK3	37.4199	29.3424	09	L.Mio.	Mudstone-marl	193/18	0082.0	1.005	1.005	1.010	0.030	189.6/05.6	283.9/37.0	092.3/52.4	191.5/06.4	283.7/19.0	083.8/69.8	31.8	29.5	28.2
	PK4	37.3402	29.3659	13	L.Mio.	Mudstone-marl	252/10	3,240.0	1.007	1.014	1.021	0.250	244.7/04.8	335.0/03.9	103.6/83.8	245.6/06.0	155.0/06.1	020.1/81.4	19.3	35.7	33.1
	EL3	37.2308	29.5361	05	Plio.	Mudstone-marl	138/23	4,660.0	1.004	1.011	1.015	0.413	063.3/05.4	154.4/11.7	308.9/77.1	065.2/27.5	157.5/04.5	256.0/62.1	20.5	20.7	06.5
	EL4	37.1866	29.5324	06	Plio.	Mudstone-marl	188/08	5,990.0	1.007	1.078	1.095	0.783	275.3/11.8	06.5/05.8	122.1/76.8	275.4/03.8	005.7/05.5	150.7/83.3	47.5	47.5	04.4
L.Mio.-Plio.	Mean	–	–	33	L.Mio.-Plio.	–	180/11	3,100.0	1.006	1.022	1.031	0.312	237.1/05.3	327.9/08.8	116.31/79.7	239.7/0.4	329.7/03.5	143.8/86.5	42	42.4	16.6
Burdur	~~BU1~~	~~37.6848~~	~~30.3129~~	~~08~~	~~Plio.~~	~~Mudstone-marl~~	~~090/20~~	~~0040.8~~	~~1.008~~	~~1.009~~	~~1.017~~	~~0.058~~	~~233.5/29.4~~	~~141.6/03.4~~	~~045.6/60.3~~	~~226.9/16.5~~	~~320.6/12.2~~	~~085.4/69.2~~	~~62.1~~	~~62.3~~	~~31.0~~
	BU2	37.6218	30.2732	10	Plio.	Mudstone-marl	070/20	0174.0	1.007	1.024	1.033	0.481	245.7/13.2	155.2/02.0	057.0/76.6	241.4/11.0	335.0/18.0	121.5/68.8	18.5	18.8	07.2
	BU3	37.5796	30.1568	06	Plio.	Mudstone-marl	355/19	0076.5	1.003	1.015	1.020	0.663	293.4/11.0	023.9/02.7	127.5/78.6	296.7/27.5	203.3/6.5	101.2/61.6	33.0	32.8	09.1
	RB1	37.7074	30.2925	15	Plio.	Mudstone-sand.	043/11	0012.0	1.019	1.024	1.045	0.167	234.7/11.9	144.5/00.6	051.6/78.1	232.2/13.8	324.7/10.2	089.8/72.7	23.9	23.9	07.5
	RB2	37.7074	30.2925	07	Plio.	Mudstone-sand.	040/16	0031.4	1.008	1.023	1.033	0.439	067.1/02.3	337.0/00.3	239.0/87.7	246.7/05.0	138.3/74.6	138.3/74.6	11.8	13.0	07.5
	SK7	37.4861	30.1595	18	Plio.	Mudstone-marl	036/16	0092.2	1.003	1.020	1.026	0.685	090.0/08.7	180.7/04.4	297.4/80.3	270.4/04.3	000.7/04.9	138.9/83.5	18.2	18.4	07.4
	~~SK8~~	~~37.6389~~	~~30.1677~~	~~09~~	~~Plio.~~	~~Mudstone-marl~~	~~312/05~~	~~0080.8~~	~~1.003~~	~~1.017~~	~~1.021~~	~~0.705~~	~~131.1/08.9~~	~~040.5/04.1~~	~~286.2/80.2~~	~~130.3/08.8~~	~~220.5/00.9~~	~~316.5/81.2~~	~~65.3~~	~~65.3~~	~~11.2~~
	~~SK9~~	~~37.7053~~	~~30.2379~~	~~08~~	~~Plio.~~	~~Mudstone-marl~~	~~035/20~~	~~0006.7~~	~~1.036~~	~~1.027~~	~~1.064~~	~~−0.137~~	~~136.2/12.8~~	~~229.9/15.8~~	~~008.9/69.5~~	~~136.2/12.8~~	~~223.5/19.9~~	~~064.1/68.9~~	~~54.8~~	~~67.3~~	~~67.4~~
	RCM1	37.4689	30.1794	10	Plio.	Mudstone	070/20	0109.0	1.002	1.018	1.022	0.830	100.9/04.9	192.7/20.1	357.9/69.3	280.8/05.5	190.5/03.0	071.8/83.7	23.1	23.2	07.8
	~~BS~~	~~37.7071~~	~~30.2926~~	~~114~~	~~Plio.~~	~~Mudstone-marl~~	~~070/10~~	~~0049.8~~	~~1.007~~	~~1.019~~	~~1.028~~	~~0.399~~	~~110.9/10.4~~	~~201.5/03.2~~	~~308.7/79.1~~	~~111.6/03.7~~	~~021.3/03.7~~	~~246.7/84.8~~	~~54.5~~	~~54.6~~	~~15.1~~
Plio.	Mean	–	–	66	Plio.	–	044/15	0081.0	1.01	1.02	1.03	0.53	243.2/05.7	152.7/04.9	022.2/82.5	241.2/09.5	332.8/09.6	107.6/76.4	35	35	10
Çameli	~~RMC3~~	~~37.0369~~	~~29.4547~~	~~20~~	~~L.Mio.-Plio.~~	~~Clay-sandstone~~	~~130/10~~	~~0010.4~~	~~1.043~~	~~1.023~~	~~1.072~~	~~−0.005~~	~~098.3/21.7~~	~~358.1/24.1~~	~~225.4/56.6~~	~~102.2/26.7~~	~~354.5/31.3~~	~~224.3/46.6~~	~~47.2~~	~~60.0~~	~~60.0~~
	~~RCM4~~	~~37.0236~~	~~29.3859~~	~~23~~	~~L.Mio.-Plio.~~	~~Mudstone-marl~~	~~220/10~~	~~0009.1~~	~~1.011~~	~~1.011~~	~~1.023~~	~~−0.023~~	~~163.4/22.8~~	~~256.8/08.1~~	~~005.3/65.6~~	~~164.7/26.9~~	~~257.3/05.1~~	~~357.2/62.5~~	~~20.6~~	~~56.5~~	~~56.2~~
	RCM5	36.9765	29.3600	17	L.Mio.-Plio.	Mudstone-marl	220/05	0325.0	1.004	1.008	1.013	0.178	233.7/07.6	324.1/03.2	077.2/81.8	234.4/04.3	144.1/04.1	011.0/84.1	36.7	37.2	20.9

Continued

Table 1
Continued

Locality	Site	Geographic coordinates (°) Latitude (N)	Longitude (E)	N_{AMS}	Age	Rock	Bedding Strike/dip	$k_m \times 10^{-6}$ (SI)	L	F	P_j	T	BTC D/I (k_1)	BTC D/I (k_2)	BTC D/I (k_3)	TC D/I (k_1)	TC D/I (k_2)	TC D/I (k_3)	e_1	e_2	e_3
	RCM6	37.0718	29.3126	59	L.Mio.-Plio.	Clay	210/08	0035.2	1.004	1.015	1.020	0.612	161.9/09.4	068.9/12.9	287.2/74.0	160.9/04.3	070.6/04.4	295.4/83.8	44.5	44.5	07.6
	RCM7	37.0602	29.2394	24	L.Mio.-Plio.	Clay	012/10	0066.1	1.004	1.018	1.024	0.659	044.4/01.5	314.3/02.4	165.8/87.1	224.4/04.2	314.7/04.2	089.7/84.0	10.5	10.5	05.7
	RCM8	37.0263	29.0185	30	L.Mio.-Plio.	Clay-sandstone	332/06	0061.9	1.002	1.014	1.017	0.703	266.1/17.9	011.0/17.9	156.6/46.0	277.1/13.4	007.5/01.6	104.3/76.5	30.8	31.0	09.1
	RCM9	36.9768	29.2231	35	L.Mio.-Plio.	Clay	265/38	0016.4	1.012	1.018	1.031	0.218	048.9/48.1	155.0/13.9	256.3/38.5	054.2/09.1	145.9/10.6	284.4/76.0	25.6	25.7	13.8
	RCM10	36.9482	29.1491	43	L.Mio.-Plio.	Clay	335/40	0067.9	1.007	1.010	1.017	0.193	086.2/19.5	182.3/16.9	310.3/63.7	268.2/00.1	178.2/05.7	359.4/84.2	11.1	11.1	06.1
	PK5	37.2315	29.3070	10	L.Mio.-Plio.	Mudstone-marl	350/18	2,320.0	1.003	1.014	1.018	0.486	280.5/12.3	011.3/03.3	116.2/77.2	283.1/29.1	191.3/03.2	095.5/60.7	29.7	30.9	20.9
	PK6	37.2099	29.3488	07	L.Mio.-Plio.	Mudstone-marl	345/10	0069.3	1.004	1.004	1.008	0.132	107.0/12.9	016.8/01.0	282.5/77.1	106.2/04.3	196.5/04.3	330.9/83.9	49.6	49.4	31.0
	SK5	37.0444	29.5360	17	L.Mio.-Plio.	Mudstone-marl	356/29	0146.0	1.005	1.006	1.010	0.093	051.8/14.8	143.8/07.5	259.7/73.3	047.9/01.8	324.0/08.2	094.3/77.5	24.9	30.8	29.6
	~~SK6~~	~~37.1036~~	~~29.5265~~	~~17~~	~~L.Mio.-Plio.~~	~~Mudstone-marl~~	~~320/08~~	~~0059.5~~	~~1.006~~	~~1.009~~	~~1.016~~	~~0.211~~	~~044.7/20.6~~	~~312.7/05.4~~	~~208.8/68.7~~	~~045.0/12.6~~	~~313.5/06.3~~	~~197.5/75.9~~	~~59.6~~	~~59.6~~	~~14.3~~
L.Mio.-Plio.	Mean	–	–	285	L.Mio.-Plio.	–	325/13	0144.0	1.008	1.014	1.022	0.346	076.8/19.5	166.9/00.3	257.9/70.5	089.1/05.1	179.2/01.2	282.28/84.8	81.0	80.0	30.1
Denizli	BD2	37.8168	28.8638	05	L.Mio.	Marl	028/16	0104.0	1.002	1.018	1.022	0.784	126.6/10.3	036.3/01.6	297.3/79.6	306.5/05.5	216.4/00.7	119.4/84.4	19.1	19.1	03.1
	~~BD3~~	~~37.7699~~	~~28.7296~~	~~12~~	~~Lt.Mio.~~	~~Limestone~~	~~118/22~~	~~0131.0~~	~~1.005~~	~~1.006~~	~~1.012~~	~~−0.029~~	~~213.4/26.3~~	~~119.2/08.4~~	~~013.0/62.2~~	~~212.8/04.3~~	~~122.3/07.3~~	~~333.4/81.5~~	~~52.1~~	~~56.7~~	~~52.2~~
	~~BD4~~	~~37.7329~~	~~28.6304~~	~~16~~	~~L.Mio.~~	~~Marl~~	~~+~~	~~0023.6~~	~~1.010~~	~~1.014~~	~~1.025~~	~~0.183~~	~~271.7/06.3~~	~~002.3/05.5~~	~~132.9/81.6~~	~~271.7/06.3~~	~~002.3/05.5~~	~~132.9/81.6~~	~~54.8~~	~~54.5~~	~~24.4~~
	BD5	37.8621	28.6718	10	L.Mio.	Marl	136/24	1,330.0	1.018	1.058	1.080	0.536	165.1/01.8	255.6/15.4	068.7/74.5	343.6/09.8	074.6/05.7	194.2/78.7	42.2	42.2	05.2
L.Mio.	Mean	–	–	15	L.Mio.	–	097/12	0924.0	1.01	1.05	1.06	0.619	164.3/02.3	254.8/12.5	63.9/77.3	339.7/08.8	070.5/05.0	190.0/79.9	47	47.1	6.3
Didim	~~DM1~~	~~37.4776~~	~~27.3436~~	~~25~~	~~Plio.~~	~~Limestone~~	~~024/12~~	~~0024.1~~	~~1.104~~	~~1.069~~	~~1.207~~	~~0.055~~	~~147.5/19.9~~	~~258.4/44.6~~	~~040.6/38.7~~	~~145.8/09.8~~	~~249.4/53.9~~	~~049.0/34.4~~	~~29.4~~	~~34.5~~	~~30.1~~
	~~DM2~~	~~37.4127~~	~~27.3755~~	~~27~~	~~Plio.~~	~~Limestone~~	~~002/07~~	~~−0006.4~~	~~1.050~~	~~1.033~~	~~1.100~~	~~−0.051~~	~~111.9/03.4~~	~~020.3/26.1~~	~~208.7/63.7~~	~~291.9/03.2~~	~~023.3/23.7~~	~~194.6/66.0~~	~~30.5~~	~~53.1~~	~~52.8~~
	DM3	37.3976	27.2433	21	Plio.	Marl	+	1,130.0	1.004	1.037	1.045	0.794	117.0/02.3	026.3/04.0	237.4/85.4	117.0/02.3	026.8/04.0	237.4/85.4	41.5	41.5	08.0
	~~DM4~~	~~37.3955~~	~~27.3511~~	~~27~~	~~Plio.~~	~~Limestone~~	~~+~~	~~0772.0~~	~~1.005~~	~~1.007~~	~~1.013~~	~~0.184~~	~~299.2/10.8~~	~~209.0/00.9~~	~~114.1/79.2~~	~~299.2/10.8~~	~~209.0/00.9~~	~~114.1/79.2~~	~~63.1~~	~~63.2~~	~~37.0~~
Plio.	Mean	–	–	21	Plio.	–	–	1,130.0	1	1.04	1.05	0.794	117.0/02.3	026.3/04.0	237.4/85.4	117.0/02.3	026.8/04.0	237.4/85.4	42	41.5	8.0
Dinar	~~BU4~~	~~38.0392~~	~~30.0896~~	~~07~~	~~Plio.~~	~~Mudstone-marl~~	~~080/11~~	~~0050.4~~	~~1.038~~	~~1.358~~	~~1.534~~	~~0.393~~	~~306.2/61.6~~	~~207.1/04.9~~	~~114.5/27.9~~	~~287.1/68.3~~	~~027.0/03.9~~	~~118.5/21.3~~	~~20.5~~	~~20.8~~	~~08.5~~
	~~SK10~~	~~37.9578~~	~~29.8946~~	~~13~~	~~Plio.~~	~~Mudstone-marl~~	~~215/06~~	~~0621.0~~	~~1.008~~	~~1.006~~	~~1.014~~	~~−0.142~~	~~039.0/84.8~~	~~283.9/02.2~~	~~193.8/04.7~~	~~347.6/82.4~~	~~103.9/003.4~~	~~194.3/06.8~~	~~27.8~~	~~33.2~~	~~28.6~~

Locality	Site	Geographic coordinates (°) Latitude (N)	Longitude (E)	N_{AMS}	Age	Rock	Bedding Strike/dip	$k_m \times 10^{-6}$ (SI)	L	F	P_j	T	BTC D/I (k_1)	BTC D/I (k_2)	BTC D/I (k_3)	TC D/I (k_1)	TC D/I (k_2)	TC D/I (k_3)	e_1	e_2	e_3
Plio.	Mean	No data available																			
Elmalı	ST1	36.4245	29.5558	28	E.-Mid. Mio.	Sandstone-mudstone	255/40	1,020.0	1.017	1.040	1.060	0.381	296.2/21.8	042.0/34.1	180.0/47.8	120.4/06.2	029.5/08.0	248.0/79.9	31.6	33.7	18.5
	ST2	36.3789	29.5091	33	E.-Mid. Mio.	Limestone	231/42	0078.0	1.007	1.018	1.026	0.390	249.6/04.5	344.2/45.4	155.3/44.2	068.0/08.9	337.1/05.6	215.4/79.4	13.1	13.0	07.4
	ST3	36.6075	29.7410	20	E.-Mid. Mio.	Limestone	185/45	0305.0	1.011	1.029	1.042	0.430	348.5/16.2	240.3/47.1	091.8/38.4	342.0/00.2	252.0/07.0	073.9/83.0	22.6	22.5	10.7
	ST4	36.3795	29.9363	22	E.-Mid. Mio.	Limestone	274/31	0083.7	1.005	1.018	1.025	0.580	300.4/05.0	031.8/15.5	193.1/73.7	119.5/08.8	211.4/12.1	354.2/74.9	15.7	15.7	06.5
	ST5	37.0515	30.1534	20	E.-Mid. Mio.	Limestone	220/40	0044.6	1.006	1.020	1.028	0.511	025.1/25.4	284.1/22.0	158.5/55.3	012.5/10.3	105.2/14.5	248.2/72.1	20.4	20.6	12.0
	~~ST6~~	~~37.0387~~	~~30.0888~~	~~09~~	~~E.-Mid. Mio.~~	~~Mudstone-marl~~	~~145/66~~	~~0440.0~~	~~1.029~~	~~1.053~~	~~1.084~~	~~0.292~~	~~181.7/01.8~~	~~272.3/17.1~~	~~085.8/72.8~~	~~343.7/32.2~~	~~100.0/35.1~~	~~223.9/38.3~~	~~03.3~~	~~03.7~~	~~03.7~~
	~~EL1~~	~~36.5159~~	~~29.6760~~	~~08~~	~~E.-Mid. Mio.~~	~~Mudstone-marl~~	~~230/32~~	~~−0004.5~~	~~1.133~~	~~1.113~~	~~1.272~~	~~−0.040~~	~~059.1/05.4~~	~~151.9/27.5~~	~~318.9/61.9~~	~~054.8/09.4~~	~~160.4/58.3~~	~~319.4/29.9~~	~~73.8~~	~~73.8~~	~~58.4~~
	EL2	36.5489	29.6611	05	E.-Mid. Mio.	Mudstone-marl	234/08	0889.0	1.033	1.053	1.089	0.228	006.1/12.1	271.9/19.2	126.4/67.0	005.3/06.1	273.7/14.2	117.8/74.5	03.4	05.2	04.2
	SK3	36.4740	29.6417	05	E.-Mid. Mio.	Mudstone-marl	220/29	0048.0	1.011	1.015	1.027	0.132	323.8/30.6	226.1/12.8	116.2/56.2	321.9/02.3	231.6/08.3	067.4/81.4	13.3	15.2	12.8
	~~SK4~~	~~36.5369~~	~~29.7052~~	~~10~~	~~E.-Mid. Mio.~~	~~Mudstone-marl~~	~~210/21~~	~~0000.2~~	~~1.153~~	~~1.265~~	~~1.496~~	~~−0.092~~	~~331.0/23.9~~	~~066.5/44.1~~	~~222.0/36.4~~	~~328.3/05.6~~	~~068.0/59.8~~	~~235.0/29.6~~	~~82.4~~	~~82.4~~	~~46.7~~
	GM	36.5308	29.6615	316	E.-Mid. Mio.	Siltstone-mudstone	220/26	0885.0	1.021	1.030	1.053	0.114	320.0/14.2	222.5/27.3	074.5/58.6	142.5/09.5	234.2/10.0	009.8/76.2	30.7	31.2	29.0
E.-Mid. Mio.	Mean	–	–	449	E.-Mid. Mio.	–	229/30	0722.0	1.018	1.028	1.049	0.214	317.5/18.7	221.7/16.7	092.8/64.5	141.7/07.2	232.4/04.9	356.1/81.3	35.8	36.2	26.5
Fethiye	~~FE1~~	~~36.7181~~	~~29.4228~~	~~09~~	~~M.Mio.~~	~~Sandstone-marl~~	~~290/35~~	~~0539.0~~	~~1.023~~	~~1.032~~	~~1.057~~	~~0.136~~	~~015.8/02.8~~	~~284.1/32.2~~	~~110.2/57.7~~	~~195.0/32.1~~	~~305.5/29.1~~	~~067.9/43.9~~	~~25.6~~	~~25.7~~	~~13.7~~
	FE2	36.7098	29.4162	13	M.Mio.	Mudstone-marl	321/20	0127.0	1.008	1.029	1.039	0.580	325.3/14.6	058.6/12.2	186.9/70.8	330.1/12.3	238.5/07.6	117.3/75.5	42.4	42.3	25.2
	FE4	36.4531	29.2902	12	Plio.	Mudstone-marl	045/20	0639.0	1.007	1.012	1.019	0.276	286.1/03.2	016.2/01.0	122.8/86.6	284.0/20.6	018.0/10.4	132.2/66.7	35.8	35.9	22.1
	~~FE6~~	~~36.3603~~	~~29.3307~~	~~05~~	~~Plio.~~	~~Mudstone-marl~~	~~045/20~~	~~0881.0~~	~~1.005~~	~~1.007~~	~~1.013~~	~~0.032~~	~~130.7/11.0~~	~~038.8/09.8~~	~~268.1/75.2~~	~~310.8/09.0~~	~~042.6/11.3~~	~~183.1/75.5~~	~~71.1~~	~~71.2~~	~~23.9~~
	SK1	36.6460	29.3980	09	M.Mio.	Mudstone-marl	215/12	0286.0	1.016	1.042	1.061	0.438	353.9/01.4	263.3/23.5	087.0/66.4	174.3/06.5	266.0/14.4	060.6/74.2	20.8	23.7	13.7
	SK2	36.4622	29.3633	08	Plio.	Mudstone-marl	000/10	3,690.0	1.009	1.075	1.093	0.740	029.6/14.9	119.6/00.3	210.9/75.1	031.5/09.8	300.0/08.4	170.2/77.1	32.3	32.3	06.1

Continued

10.1029/2021TC006882

Table 1
Continued

		Geographic coordinates (°)					Bedding						BTC			TC					
Locality	Site	Latitude (N)	Longitude (E)	N_{AMS}	Age	Rock	Strike/dip	$k_m \times 10^{-6}$ (SI)	L	F	P_j	T	D/I (k_1)	D/I (k_2)	D/I (k_3)	D/I (k_1)	D/I (k_2)	D/I (k_3)	e_1	e_2	e_3
Plio.	Mean	–	–	20	Plio.	–	030/14	1,860.0	1.01	1.04	1.05	0.462	081.7/07.4	350.3/10.3	206.7/77.3	062.1/01.8	331.6/14.4	158.9/75.5	75	74.9	12.0
M. Mio.		–	–	22	M.Mio.	–	286/10	0192.0	1.01	1.03	1.05	0.522	342.7/10.9	251.3/07.2	128.6/76.9	349.9/01.2	259.6/13.5	084.7/76.5	39	38.2	21
Ören	OR1	37.1673	27.8175	12	E.-Mid. Mio.	Mudstone-marl	089/05	0023.3	1.011	1.012	1.030	−0.187	157.5/07.6	249.0/11.3	034.0/76.3	157.6/03.0	248.1/9.5	050.4/80.0	30.6	35.5	35.4
	~~OR2~~	~~37.1533~~	~~27.8866~~	~~07~~	~~E.-Mid. Mio.~~	~~Sandstone-marl~~	~~153/32~~	~~−0005.7~~	~~1.087~~	~~1.079~~	~~1.185~~	~~0.119~~	~~126.7/49.3~~	~~300.67/40.6~~	~~033.2/03.0~~	~~168.0/52.8~~	~~285.9/19.6~~	~~027.9/30.2~~	~~45.6~~	~~45.9~~	~~21.1~~
	~~OR3~~	~~37.0757~~	~~27.9431~~	~~08~~	~~E.-Mid. Mio.~~	~~Mudstone-marl~~	~~344/18~~	~~−0008.8~~	~~1.041~~	~~1.075~~	~~1.123~~	~~0.294~~	~~317.2/47.7~~	~~225.6/01.5~~	~~134.3/42.3~~	~~338.3/52.8~~	~~224.2/17.2~~	~~123.1/31.8~~	~~66.7~~	~~65.6~~	~~41.7~~
	~~OR4~~	~~37.0473~~	~~28.0191~~	~~11~~	~~E.-Mid. Mio.~~	~~Mudstone-marl~~	~~260/18~~	~~−0002.4~~	~~0.970~~	~~1.008~~	~~1.144~~	~~−0.194~~	~~006.4/20.3~~	~~100.3/17.2~~	~~230.2/62.9~~	~~005.4/03.0~~	~~096.7/23.4~~	~~268.6/66.6~~	~~18.9~~	~~23.8~~	~~25.4~~
	~~OR5~~	~~37.0582~~	~~28.1703~~	~~13~~	~~E.-Mid. Mio.~~	~~Mudstone-marl~~	~~290/10~~	~~0074.9~~	~~1.016~~	~~1.023~~	~~1.040~~	~~0.196~~	~~215.6/06.4~~	~~123.2/20.0~~	~~322.6/68.9~~	~~216.1/16.1~~	~~119.5/22.0~~	~~339.3/62.3~~	~~12.9~~	~~14.5~~	~~13.7~~
	OR6	37.1838	27.8378	09	E.-Mid. Mio.	Mudstone-marl	203/17	0620.0	1.003	1.003	1.006	0.110	295.6/03.1	205.4/05.0	057.6/84.2	115.7/13.9	206.7/04.0	312.6/75.5	43.5	44.9	36.5
	~~YT1~~	~~37.2353~~	~~28.1945~~	~~04~~	~~E.-Mid. Mio.~~	~~Mudstone-marl~~	~~075/11~~							~~No data available~~							
	~~YT2~~	~~37.2632~~	~~28.1083~~	~~02~~	~~E.-Mid. Mio.~~	~~Mudstone-marl~~	~~000/12~~							~~No data available~~							
	~~YT3~~	~~37.3641~~	~~28.0549~~	~~11~~	~~E.-Mid. Mio.~~	~~Mudstone-marl~~	~~305/08~~	~~0030.3~~	~~1.024~~	~~1.069~~	~~1.100~~	~~0.492~~	~~310.9/07.6~~	~~041.2/02.3~~	~~147.9/82.1~~	~~311.9/06.7~~	~~221.3/05.7~~	~~091.2/81.2~~	~~55.1~~	~~55.1~~	~~08.3~~
E.-Mid. Mio.	Mean	–	–	21	E.-Mid. Mio.	–	186/8	0279.0	1.011	1.008	1.019	−0.06	155.9/06.9	247.2/10.8	033.8/77.1	156.2/03.8	246.7/06.8	037.5/82.2	38	39.2	38
Tavas	~~TVS1~~	~~37.6254~~	~~29.0066~~	~~32~~	~~L.Mio.~~	~~Sandstone-marl~~	~~–~~	~~1,650.0~~	~~1.003~~	~~1.006~~	~~1.009~~	~~0.370~~	~~158.5/02.1~~	~~248.5/00.6~~	~~355.4/87.8~~	~~158.5/02.1~~	~~248.5/00.6~~	~~355.4/87.8~~	~~77.0~~	~~77.0~~	~~18.4~~
	TVS2	37.5142	28.8237	28	L.Mio.	Mudstone-marl	203/31	1,690.0	1.010	1.027	1.039	0.425	287.3/16.2	193.4/13.2	066.2/68.9	107.4/14.6	201.7/16.2	337.4/67.9	15.7	16.0	09.9
	~~TVS3~~	~~37.5581~~	~~28.7865~~	~~22~~	~~L.Mio.~~	~~Mudstone-marl~~	~~–~~	~~1,230.0~~	~~1.001~~	~~1.002~~	~~1.003~~	~~0.090~~	~~067.7/07.4~~	~~337.2/03.9~~	~~219.5/81.6~~	~~067.7/07.4~~	~~337.2/03.9~~	~~219.5/81.6~~	~~60.2~~	~~60.2~~	~~34.9~~
	~~TVS4~~	~~37.5345~~	~~28.6366~~	~~20~~	~~L.Mio.~~	~~Mudstone-marl~~	~~–~~	~~−0002.9~~	~~3.040~~	~~1.111~~	~~1.332~~	~~0.192~~	~~172.4/76.3~~	~~285.1/05.4~~	~~016.3/12.6~~	~~172.4/76.3~~	~~285.1/05.4~~	~~016.3/12.6~~	~~27.0~~	~~36.4~~	~~31.4~~
	~~TVS5~~	~~37.4681~~	~~28.6498~~	~~16~~	~~L.Mio.~~	~~Limestone~~	~~142/06~~	~~0095.7~~	~~1.012~~	~~1.042~~	~~1.057~~	~~0.560~~	~~330.0/14.1~~	~~060.5/02.2~~	~~159.3/75.7~~	~~328.4/14.9~~	~~060.6/08.2~~	~~178.5/73.0~~	~~58.9~~	~~58.8~~	~~10.7~~
	KL1	37.2711	28.6523	12	Ol.-E. Mio.	Mudstone-marl	158/26	0341.0	1.005	1.019	1.025	0.569	171.6/40.4	078.9/03.2	345.1/49.4	189.0/30.3	080.4/28.7	316.0/45.8	06.4	06.4	03.0
	~~KL2~~	~~37.2707~~	~~28.6187~~	~~17~~	~~Ol.-E. Mio.~~	~~Mudstone-marl~~	~~044/55~~	~~1,110.0~~	~~1.007~~	~~1.092~~	~~1.112~~	~~0.853~~	~~206.8/32.4~~	~~078.1/44.6~~	~~316.5/28.0~~	~~188.2/05.9~~	~~097.7/04.3~~	~~331.7/82.7~~	~~56.1~~	~~56.0~~	~~10.1~~
	KL3	37.2773	28.6246	29	E.Mio.	Mudstone-marl	056/34	2,260.0	1.004	1.052	1.063	0.858	210.1/30.6	099.4/31.0	334.5/43.6	198.4/12.2	107.2/05.6	353.2/76.5	26.5	26.6	06.2

		Geographic coordinates (°)					Bedding						BTC			TC					
Locality	Site	Latitude (N)	Longitude (E)	N_{AMS}	Age	Rock	Strike/dip	$k_m \times 10^{-6}$ (SI)	L	F	P_j	T	D/I (k_1)	D/I (k_2)	D/I (k_3)	D/I (k_1)	D/I (k_2)	D/I (k_3)	e_1	e_2	e_3
	KL4	37.3237	28.6275	21	Ol.-E. Mio.	Mudstone-marl	310/26	1,210.0	1.023	1.077	1.107	0.522	343.2/05.6	076.1/27.4	242.62/61.9	162.6/08.7	308.8/79.6	308.8/79.6	05.5	05.5	03.7
	~~KL5~~	~~37.3719~~	~~28.5949~~	~~20~~	~~E.Mio.~~	~~Mudstone-marl~~	~~214/11~~	~~0647.0~~	~~1.004~~	~~1.021~~	~~1.027~~	~~0.698~~	~~187.3/05.5~~	~~097.1/01.3~~	~~353.6/84.3~~	~~188.7/10.4~~	~~096.6/11.1~~	~~320.6/74.7~~	~~69.9~~	~~69.9~~	~~9.1~~
	~~KL6~~	~~37.3673~~	~~28.6562~~	~~16~~	~~E.Mio.~~	~~Mudstone-marl~~	~~202/11~~	~~0011.1~~	~~1.071~~	~~1.103~~	~~1.192~~	~~0.305~~	~~328.7/08.1~~	~~237.2/10.6~~	~~095.3/76.6~~	~~328.7/08.1~~	~~238.3/04.2~~	~~048.1/85.8~~	~~54.9~~	~~54.8~~	~~24.2~~
L.Mio.	Mean	–	–	28	L.Mio.	–	203/31	1,690.0	1.010	1.03	1.04	0.425	287.3/16.2	193.4/13.2	066.2/68.9	107.4/14.6	201.7/16.2	337.4/67.9	16	16	9.9
Ol.-E. Mio.		–	–	62	Ol.-E. Mio.	–	058/08	1,540.0	1.01	1.05	1.07	0.688	122.5/25.6	031.6/01.9	297.5/64.3	171.9/11.8	080.9/04.5	330.3/77.3	24	23.7	6.7
Ulubey	~~PK1~~	~~38.0081~~	~~29.1435~~	~~12~~	~~Plio.~~	~~Sandstone-marl~~	~~304/09~~	~~0021.8~~	~~1.028~~	~~1.022~~	~~1.052~~	~~−0.040~~	~~333.0/13.6~~	~~065.5/10.2~~	~~191.3/72.9~~	~~333.0/13.6~~	~~065.0/02.5~~	~~170.3/80.6~~	~~52.1~~	~~50.8~~	~~41.8~~
	CL1	37.8167	29.2797	14	Plio.	Mudstone-marl	136/16	0414.0	1.010	1.026	1.038	0.415	194.7/08.3	285.5/05.8	050.1/79.8	014.9/5.4	105.1/02.4	218.9/84.1	23.1	23.2	9.6
	~~CL2~~	~~38.3445~~	~~29.5783~~	~~13~~	~~Plio.~~	~~Mudstone-marl~~	~~+~~	~~0023.1~~	~~1.016~~	~~1.018~~	~~1.036~~	~~0.035~~	~~309.5/70.1~~	~~177.4/13.6~~	~~83.9/14.2~~	~~309.5/70.1~~	~~177.4/13.6~~	~~83.9/14.2~~	~~51.9~~	~~58.6~~	~~57.5~~
	CL3	38.5414	29.6563	15	Plio.	Limestone	057/08	2,280.0	1.006	1.022	1.029	0.477	053.7/01.2	143.8/07.2	314.5/82.7	053.9/1.6	323.9/00.8	206.6/88.2	37.3	37.2	14.6
	~~UL1~~	~~38.3454~~	~~29.2171~~	~~12~~	~~Plio.~~	~~Limestone~~	~~+~~	~~0009.1~~	~~1.100~~	~~1.145~~	~~1.291~~	~~−0.111~~	~~117.0/11.5~~	~~359.6/66.2~~	~~211.4/20.5~~	~~117.0/11.5~~	~~359.6/66.2~~	~~211.4/20.5~~	~~46.5~~	~~62.6~~	~~62.2~~
	~~UL2~~	~~38.4193~~	~~29.2599~~	~~8~~	~~Plio.~~	~~Marl~~	~~+~~	~~−0004.7~~	~~1.055~~	~~1.076~~	~~1.142~~	~~0.010~~	~~75.00/37.1~~	~~187.6/26.9~~	~~303.8/41.1~~	~~75.00/37.1~~	~~187.6/26.9~~	~~303.8/41.1~~	~~47.9~~	~~47.9~~	~~45.1~~
	UL4	38.3245	29.1011	15	Plio.	Mudstone-marl	+	2,090.0	1.005	1.035	1.044	0.576	222.3/04.1	132.0/05.3	349.9/83.2	222.3/4.1	132.0/05.3	349.9/83.2	25.7	25.7	7.3
	~~UL5~~	~~38.1230~~	~~29.0384~~	~~15~~	~~Plio.~~	~~Sandstone-marl~~	~~136/10~~	~~−0009.2~~	~~1.070~~	~~1.054~~	~~1.139~~	~~0.111~~	~~280.0/16.9~~	~~182.7/22.7~~	~~043.4/61.6~~	~~278.0/10.9~~	~~185.0/15.3~~	~~042.1/71.1~~	~~28.8~~	~~19.9~~	~~30.5~~
	UL6	38.0457	28.9604	13	Plio.	Sandstone-marl	+	1,800.0	1.003	1.003	1.006	−0.057	160.2/22.0	307.9/64.5	065.1/12.3	160.2/22.0	307.9/64.5	065.1/12.3	39	39.1	17.3
Plio.	Mean	–	–	57	Plio.	–	112/10	1,660.0	1.01	1.022	1.028	0.366	198.4/06.5	108.3/01.4	006.1/83.3	200.2/00.3	110.2/01.9	300.3/88.1	47	46.6	12
Regional																					
L.Mio.-Plio.	Mean	–	–	525	L.Mio.-Plio.	–	–	0696.0	1.01	1.019	1.029	0.404	073.7/03.1	163.7/01.2	274.6/86.7	073.8/01.1	343.8/00.2	241.3/88.9	78.8	78.8	24.7
Ol.-Mid. Mio.	Mean	–	–	551	Ol.-M. Mio.	–	–	0780.0	1.02	1.031	1.050	0.270	322.4/12.1	229.4/13.4	093.1/71.8	145.6/07.8	236.1/03.9	352.6/81.2	38.0	38.2	22.5

Note. Geographic coordinates use WGS84 datum. Strikethrough text indicates unusable/discarded sites. N_{AMS}, number of studied samples at location. k_m, mean susceptibility in 10^{-6} SI. Magnetic lineation (L), magnetic foliation (F), corrected anisotropy degree (P_j), and shape factor (T) according to Jelínek (1978). D and I are the mean declination and inclination of the maximum (k_{max}), intermediate (k_{int}), and minimum (k_{min}) susceptibility axis, respectively. $e1$, $e2$, and $e3$ semiangle of the 95% confidence ellipse around the declination of the mean maximum, intermediate, and minimum susceptibility axes, respectively. L., Late; E., Early; Ol., Oligocene; Mio., Miocene; Plio.: Pliocene

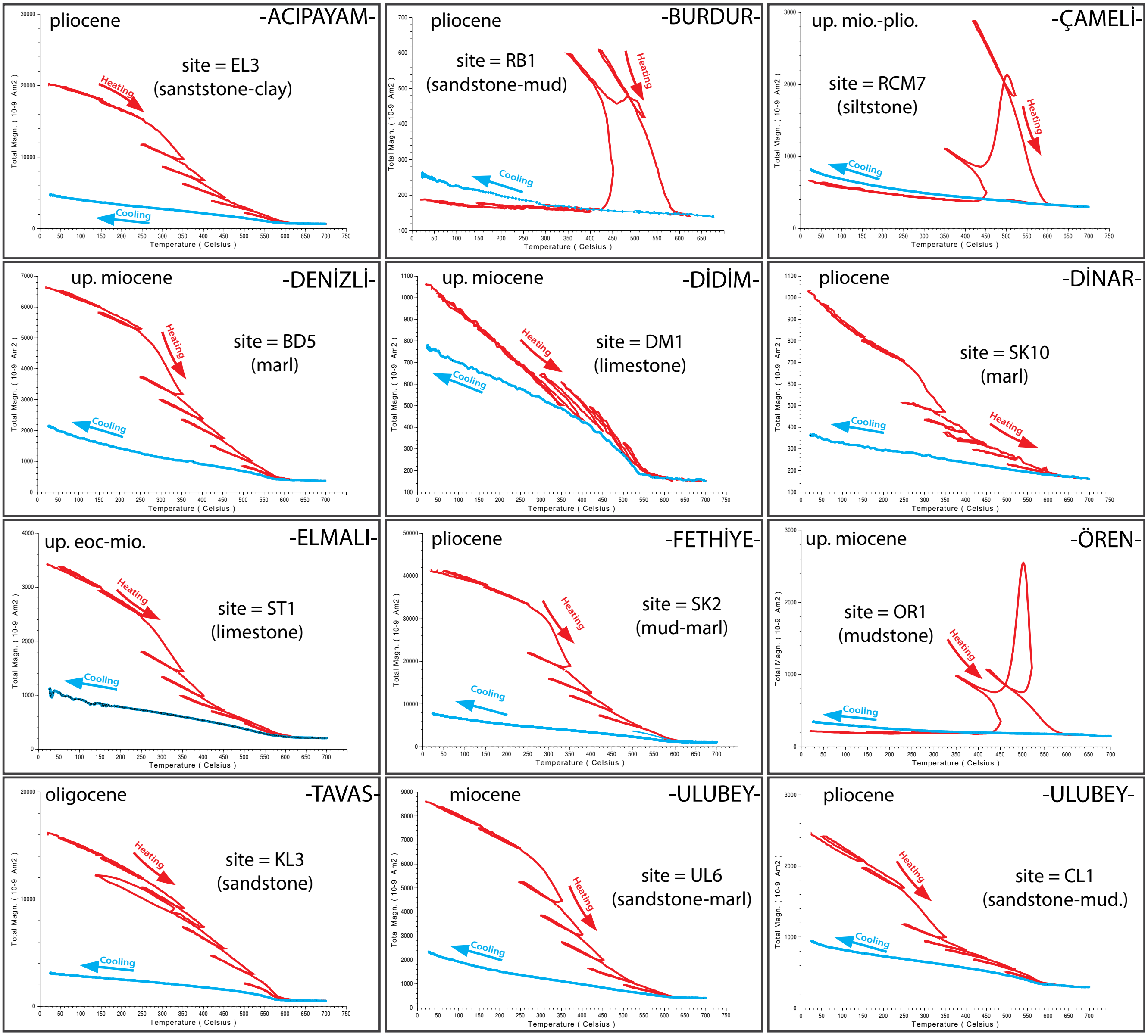

Figure 2. Representative thermomagnetic curves for samples from each site, consisting of several heating-cooling cycles to assess changes (alterations) in the magnetic properties (Mullender et al., 1993). The final cooling curve is indicated with the blue line. See the text for an explanation of the thermomagnetic behavior.

by converting from specimen coordinates to geographic and tectonic coordinates. The site mean AMS parameters were calculated according to Jelinek statistics (Jelínek, 1977, 1978), and tilt corrected results are given in Table 1.

2.4. AMS and Deformation

During the past few decades, the magnetic fabric of a rock matrix has been increasingly used as a rock deformation indicator, especially in rocks from sedimentary basins (e.g., Borradaile, 1991; Hrouda, 1991, 1993; Maffione et al., 2012; Özkaptan & Gülyüz, 2019; Parés et al., 1999; Sagnotti et al., 1994; Soto et al., 2009; Tarling & Hrouda, 1993; Wasoo et al., 2020). The magnetic fabric orientations can often identify the deformation history of sedimentary rocks, even lacking clear strain markers for low to moderately deformed areas change in for weakly to moderate deformed sedimentary deposits (e.g., Cifelli et al., 2005, 2004; Graham, 1966; Hirt et al., 1995; Kissel et al., 1986; Kodama, 1995; Mattei et al., 1997).

The AMS ellipsoid is described by a tensor, which is defined by three principal axes; $k_1 \geq k_2 \geq k_3$ that refer to maximum, intermediate, and minimum susceptibility, respectively (Hrouda, 1982). The shape of the magnetic ellipsoid is controlled by a combination of these three principal susceptibility vectors. A purely sedimentary fabric is characterized by a minimum axis k_3 that is perpendicular to bedding due to compaction. Because we have fine-grained sedimentary rocks and have observed no sedimentary structures due to transport direction (paleocurrents), the k_1 and k_2 axes are then randomly distributed in the horizontal bedding plane (Scheepers & Langereis, 1994). Upon compression or extension, the k_1 and k_2 axes will tend to cluster, causing a tectono-sedimentary fabric. In terms of structural observations, previous AMS studies commonly inferred that in compressional settings the k_1 axis is oriented to be perpendicular to the shortening direction and (sub)parallel to fold axes or strikes of thrust faults, while k_3 remains normal to the bedding plane (e.g., Borradaile & Henry, 1997; Graham, 1966; Maffione et al., 2015; Mattei et al., 1997; Özkaptan & Gülyüz, 2019). However, in extensional settings, the magnetic lineation vector (k_1) typically coincides with the bedding dip direction and stretching direction, and is perpendicular to strikes of local normal faults (Cifelli et al., 2005; Mattei et al., 1997, 1999; Sagnotti et al., 1994). All the measurements were corrected for bedding attitude, and AMS parameters at both the specimen and site-level were computed following the Jelinek statistics (Jelínek, 1977, 1978).

In addition to three magnetic susceptibility axes, several parameters have been used to quantify the degree of anisotropy and the shape of the magnetic ellipsoids, which are closely related to lithological features and tectonic deformation. The most commonly used ones are:

$$k_m(\text{mean magnetic susceptibility}) = (k_1 + k_2 + k_3)/3$$

$$P_j(\text{corrected anisotropy degree}) = exp\sqrt{2(n1 - n)^2 + (n2 - n)^2(n3 - n)^2}$$

$$L(\text{magnetic foliation})k_1/k_2$$

$$F(\text{magnetic foliation}) = k_2/k_3$$

$$T(\text{shape parameter}) = (2n2 - n1 - n3)/(n1 - n3)$$

where, $n = \ln k_i$, $n = (n1 + n2 + n3)/3$, as proposed by Jelínek (1981).

k_m provides mostly qualitative information about the magnetic (ferromagnetic, paramagnetic, and diamagnetic) mineral composition; P_j provides information about the elongation (prolate) or flattening (oblate) of the magnetic fabric which is assumed to be a function of strain ellipsoid (Borradaile, 1988; Parés & van der Pluijm, 2002); T is the shape factor and provides information about the shape the susceptibility ellipsoid varying between prolate (−1) and oblate (1; Ferré, 2002).

3. Results

3.1. Thermomagnetic Data

Examples of thermomagnetic runs of samples from 11 different domains, and variable rock types of Oligocene to Pliocene age are illustrated in Figure 2. In general, thermomagnetic curves present a moderately high total magnetization typically in the range $1–3 \times 10^{-6}$ Am^2 for the white marls, mud-siltstones, and limestones, whereas some gray marls and sandstones are stronger, in the range $7–30 \times 10^{-6}$ Am^2. Most curves are fully reversible up to 300°C. Above 300°C, there is an increased loss of magnetization, causing an inflection in magnetization between 300°C and 400°C. This could be due to the presence of some maghemite (Dankers, 1978; e.g., through low-temperature oxidation/weathering of magnetite), or caused by a relatively Ti-rich magnetite with a lower Curie temperature. The final cooling bulk susceptibility is significantly lower than the heating curves, indicating progressive oxidation of magnetite at the highest temperatures (700°C). Most curves show a Curie temperature of 550°C–580°C, indicative of Ti-poor magnetite. Some curves for clay-sandstone, siltstone or mudstone (RB1, RCM7, and OR1 in Figure 2) show a strong increase starting at ∼400°C which is typically an indicator for the presence of pyrite that is transformed to magnetite during thermal demagnetization, and the newly formed magnetite is subsequently demagnetized or oxidized at ∼550°C (Passier et al., 2001)

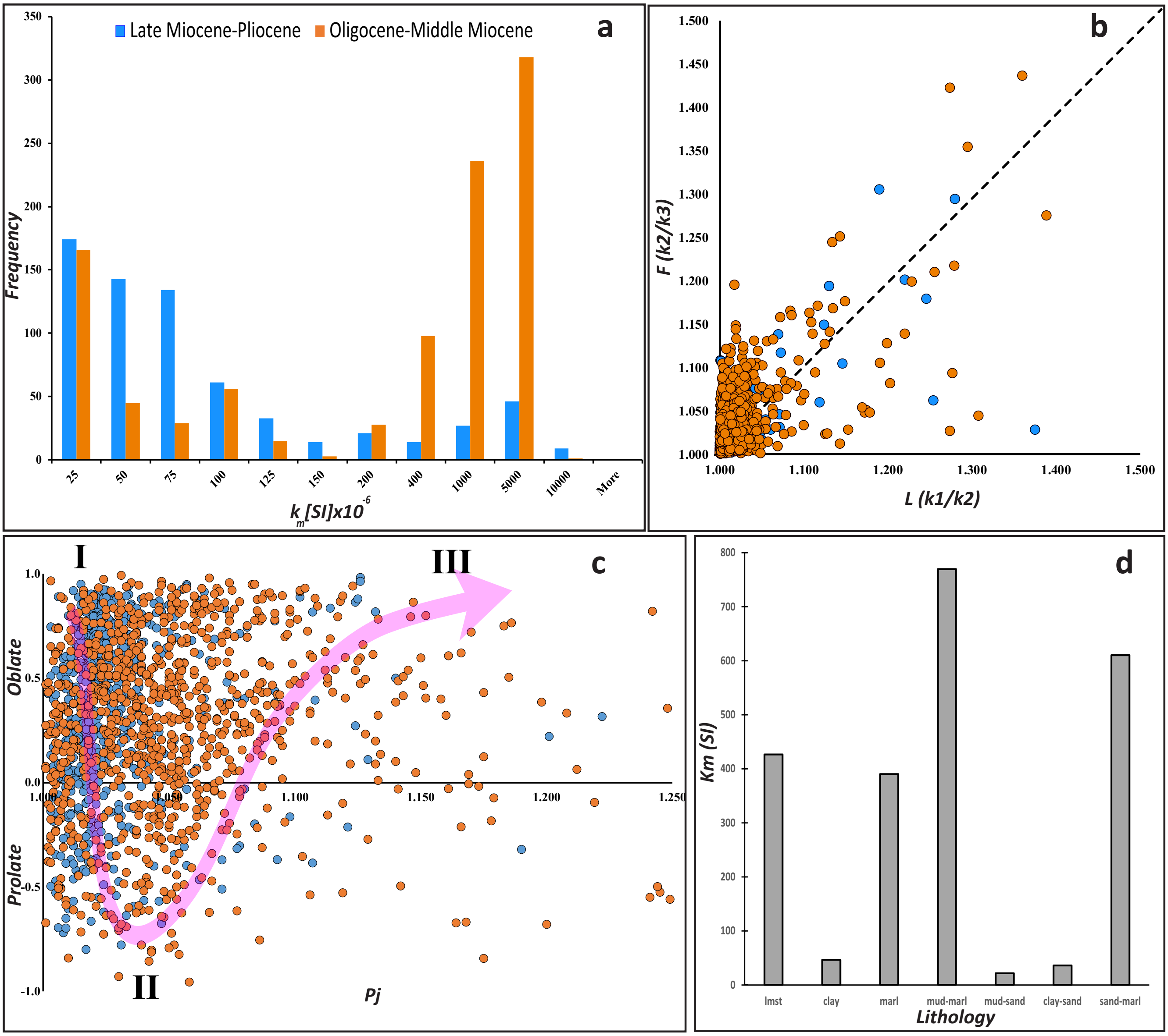

Figure 3. (a) Frequency distribution of the magnetic susceptibility (k_m) from all measured specimens. (b) Anisotropy plots of magnetic foliation (F) versus magnetic lineation ratios (L). (c) Shape factor (T) versus corrected anisotropy degree (P_j) diagram compared to the typical trend expected from an increasing degree of deformation, from an oblate sedimentary magnetic fabric (I) to a prolate tectonic-sedimentary fabric (II) and finally to an oblate purely tectonic fabric (III; e.g., Borradaile & Henry, 1997; Parés & van der Pluijm, 2004; Robion et al., 2007). (d) Lithology distribution of the magnetic susceptibility (km) from all measured sites.

3.2. AMS Data

All the AMS data obtained have been passed through strict criteria to assess their reliability and quality. The first and the most determining criterion for all sites with estimated confidence ellipses (e_1, e_2, or e_3) higher than 45° around the declination of the three susceptibility axes were rejected. The second criterion involved all sites with negative bulk susceptibility (k_m) due to diamagnetism and these were also rejected. Due to insufficient measurements ($N < 5$) two sites (YT1 and YT2) were rejected. One site (ÖR5) shows relatively high k_m (74.9×10^{-6} SI) and low e values ($e < 45°$), and k_3 is not normal (62.3°) to the bedding plane, therefore it is also rejected. The equal-area projections of the axes of the remaining AMS ellipsoids from each of the accepted 46 sites after bedding plane correction are illustrated in Figures 3 and 4. In total, 36 sites that failed to meet our criteria were excluded from the database (Figure 4 and Table 1). Subsequently, the site-based results were combined into the

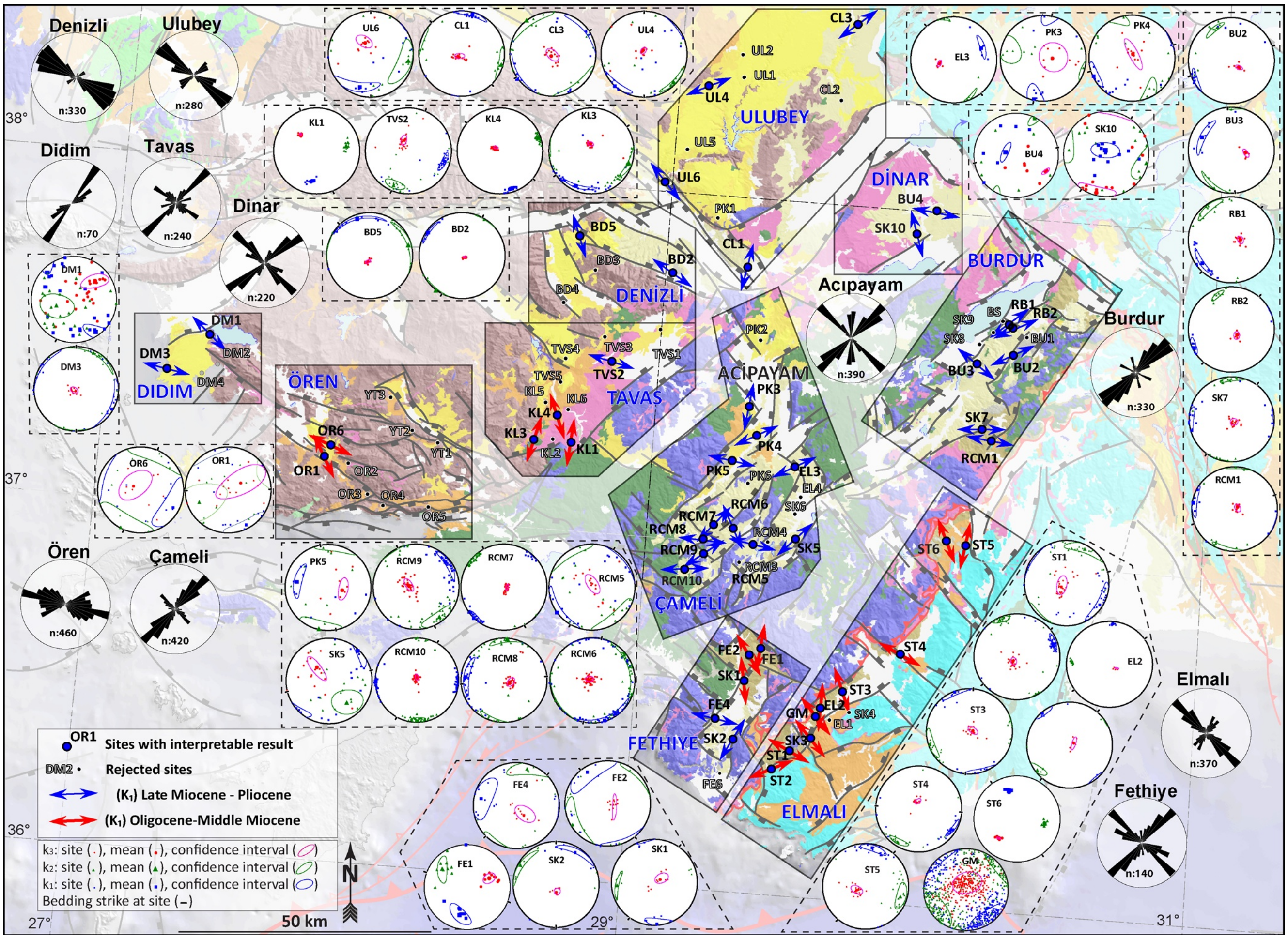

Figure 4. Lower hemisphere equal area plots of tilt corrected AMS data per site and their site mean AMS lineations. Rose diagrams are prepared from the strikes of faults within each domain.

11 different domains according to their geologic and geographic locations. The obtained results (Figure 4) are compared with the strikes of the previously mapped normal faults (Kaymakcı et al., 2018) in each domain.

3.2.1. Acıpayam Domain

The Acıpayam Domain is characterized mainly by NE-SW striking normal faults and few NW-SE striking orthogonal faults developed under multi-directional extension dominated by a NE-SW direction. The domain is represented by five sites in upper Miocene to Pliocene strata, and sampled rocks include mudstones, marls, and limestones (Table 1). The limestone site (PK2) and marl site EL4 have very low magnetic susceptibility and very large confidence ellipses ($e > 45°$) around k_1, k_2, and k_3. Therefore, these sites are rejected for further analysis (Table 1). The remaining upper Miocene (PK3 and PK4) and Pliocene rocks (EL3) indicate NNE-SSW to WNW-ESE orientations of maximum anisotropy axes (magnetic lineations). The magnetic lineations in the sites EL3, PK4 are almost perpendicular to the strikes of the nearby normal faults, whereas site PK3 yields an angle of almost 45° with the nearby orthogonal normal faults (Figure 3). The combined analysis of the four accepted sites comprises 33 specimens, and they altogether indicate a magnetic lineation oriented in 240N/00 direction after tilt correction, which is almost parallel to orientations (237N/05) before tilt correction (Figures 4–6 and Table 1).

3.2.2. Burdur Domain

The Burdur Domain is characterized mainly NE-SW striking normal faults developed under multi-directional extension dominated by about an E-W direction (Özkaptan et al., 2018). The domain is represented by 10 sites (Figure 4) where Pliocene sandstone-claystone and marl-mudstone are collected from its eastern parts (Figure 1).

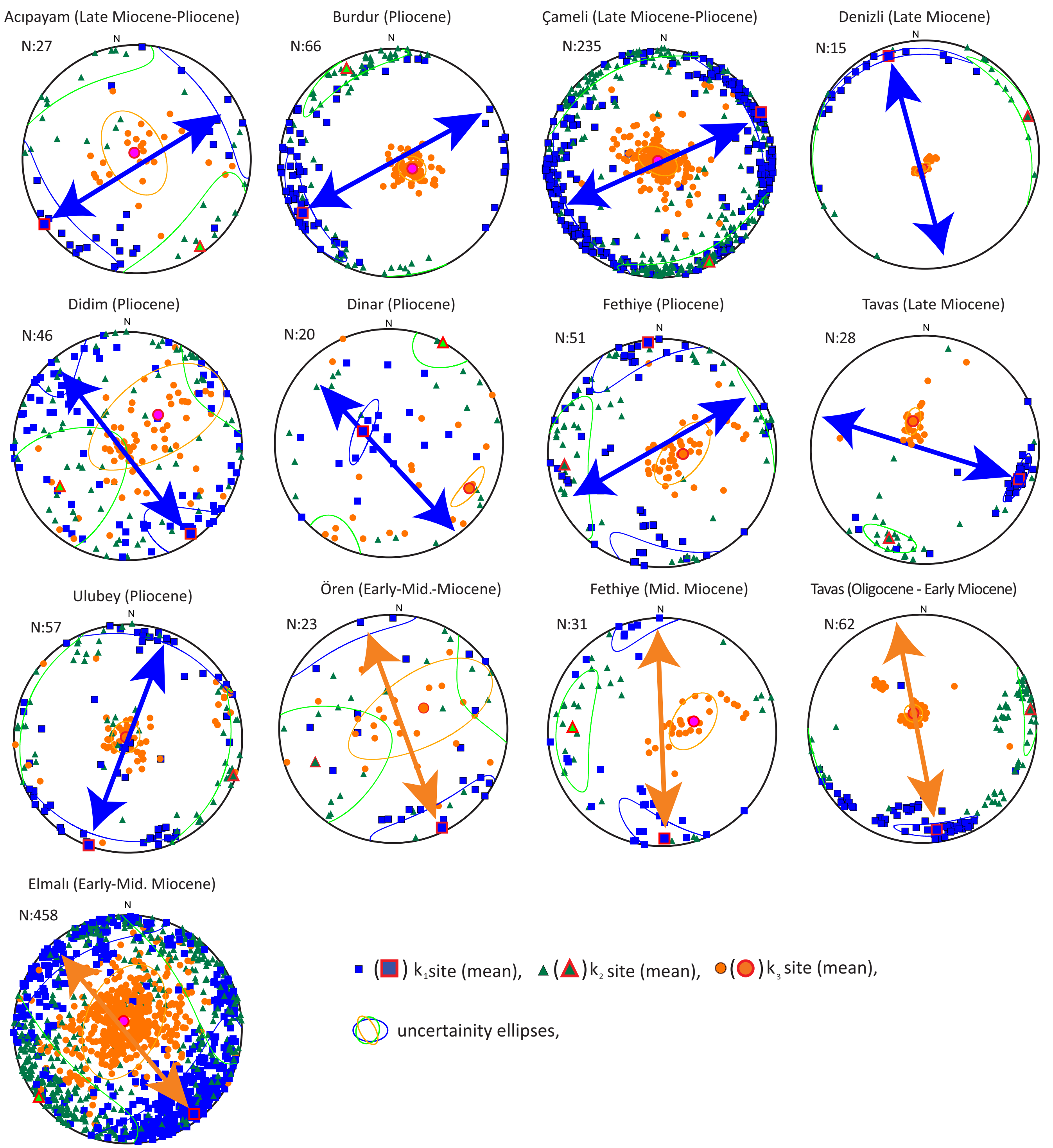

Figure 5. Lower hemisphere equal area plots of the three axes of the AMS ellipsoids from the 11 domains after bedding plane correction. The site-based AMS results are given in Table 1.

These sites have low to moderate mean magnetic susceptibility values varying between 6.7 and 174 × 10^{-6} (SI; Table 1). In sites BU1, SK8, and SK9 AMS directions are scattered and have large confidence intervals >45°. Therefore, they are rejected (Table 1). Site BS belongs to a magnetostratigraphic sampling site (Özkaptan et al., 2018). Therefore, it contains a very large number of samples, and despite the fact that the site indicates NW-SE oriented lineation, it is rejected because confidence angles are larger than 45°.

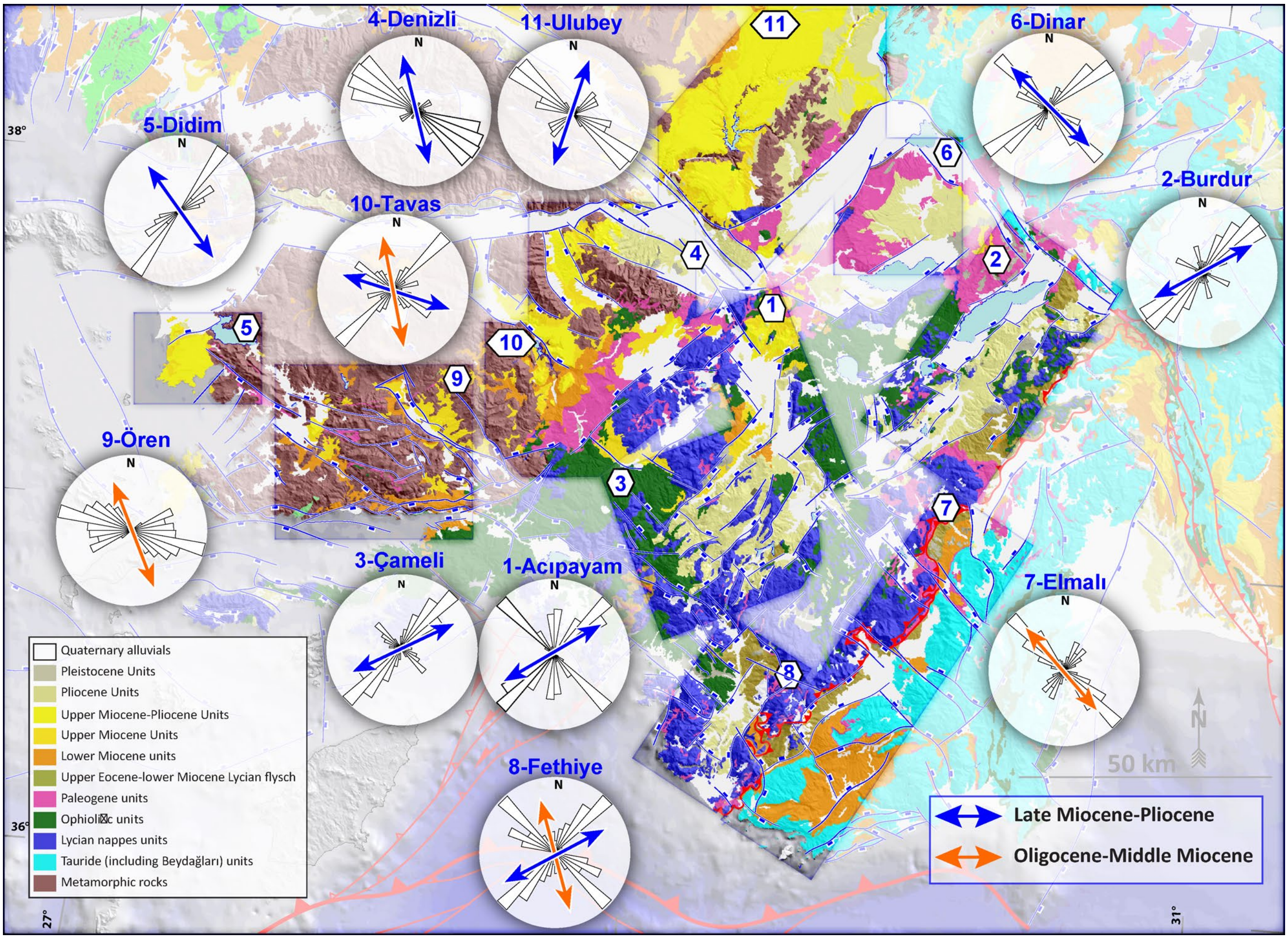

Figure 6. Orientations of the mean magnetic lineation (k_1) of each 11 domains after tectonic correction overlain on length weighted rose diagrams showing the strike of normal faults identified in each domain.

The remaining results show that magnetic lineations are oriented dominantly in two directions. In the sites, BU3 and RCM1 magnetic lineations are oriented NW-SE, whereas they are oriented NE-SW in sites BU2, BU1, RB2, and RB1 and E-W in the site SK7 (Figure 4 and Table 1). The combination of all accepted sites (66 specimens) yields k_1 oriented in 243N *in situ* and 241N (N61E) after tilt correction (Figure 5). The site mean magnetic lineations are generally parallel to the local bedding strikes. Furthermore, the strikes of the normal faults in the Burdur Domain are oriented dominantly in NE-SW, subparallel to the obtained mean magnetic lineation direction although they are almost perpendicular to orthogonal NW-SE striking short faults in the domain (Figure 6).

3.2.3. Çameli Domain

The Çameli Domain is characterized by NE-SW striking, west-facing, normal faults that developed under the NW-SE oriented extension that produced a series of west-thinning half grabens and associated fluvio-lacustrine deposits (Alçiçek et al., 2005). The domain includes 12 sites collected from upper Miocene to Pliocene marl, sandstone, mudstone intercalations, and claystone (Table 1). Two sites (RCM3 and RCM4) have very low mean magnetic susceptibility values of $\sim 10 \times 10^{-6}$ (SI), and large confidence ellipses (>45°) and are rejected. In addition, despite sites PK6 and SK6 have relatively high magnetic susceptibility values, however they have large confidence angles (e_1, $e_2 > 45$) therefore they are rejected from the database. The remaining eight sites have at least $k_m \sim 10 \times 10^{-6}$ (SI), but one site (PK5) has extremely high mean magnetic susceptibility values reaching up to $2{,}320 \times 10^{-6}$ (SI; Table 1).

Similar to the Burdur Domain, the magnetic lineations in the Çameli Domain are also oriented in two dominant directions. The first group includes the sites RMC6, RCM8, PK5, PK6, whose magnetic lineations are oriented, in general, NW-SE. The remaining sites show that k_1 is generally oriented NE-SW (Figure 3). It is important to note here that there is no age or tectonic setting difference between these sites. In addition, the AMS results from all sites do not show any significant discrepancy in both *in situ* and tilt corrected coordinates (Figures 4 and 5 and Table 1) due to their orthogonal nature with respect to bedding attitudes. Specifically, the bedding plane strikes are almost perpendicular or parallel to one of the AMS axes, except for site RCM5.

The combined analysis (235 specimens) of eight sites indicates that k_1 is oriented E-W and k_2 is oriented N-S. This orientation is almost parallel to the trends of the major normal faults in the domain (Figures 5 and 6).

3.2.4. Denizli Domain

The Denizli Domain comprises the Denizli Basin and its surroundings. The basin is characterized dominantly by NW-SE striking normal faults and NE-SW oriented relatively short but tectonically significant normal faults. According to a detailed kinematic study (Kaymakcı, 2006), the basin experienced multi-directional extensional deformation with triaxial-strain conditions. The infill of the basin is dominated by various lacustrine phases of late Miocene to Pliocene age rocks, which gradually becomes a fluvio-lacustrine environment associated with fan-deltas.

The Denizli Domain is represented by four sites in late Miocene to Pliocene age rocks (BD2, BD3, BD4, and BD5) composed of clayey-limestone and marls. The limestone site (BD3) yielded scattered directions with a very large confidence interval (>45°) for all three AMS axes (Table 1). Therefore, it is rejected and not used for further analysis. Furthermore, site BD4 has large confidence ellipses (e_1, $e_2 > 45°$) and was rejected. Both sites show that magnetic lineations are oriented ∼NW-SE and strikes of the local bedding planes are perpendicular (BD2) or subparallel (BD5) to the direction of the magnetic lineations. The combined analysis of marl bearing sites (BD2 and BD5, in total 15 specimens) indicates a magnetic lineation of ∼NW-SE (164N *in situ* and 340N after tilt correction; Figure 4 and Table 1). This orientation is sub-parallel to the trends of the dominant normal faults in the domain (Figures 5 and 6).

3.2.5. Didim Domain

The Didim Domain comprises Pliocene lacustrine deposits, which are locally cut by NE-SW striking normal faults. It is located at the southern flank of the Büyük Menderes Graben (BMG). The lacustrine deposits in the domain have been uplifted along the southern boundary fault of BMG (Figure 1b) and the NW-SE striking faults that delimit the Pliocene deposits in the east, where they are juxtaposed with the rocks of the Menderes Core Complex.

The Didim Domain contains four sites sampled in Pliocene limestones and marls. The limestone sites (DM2 and DM4) were rejected due to large scattered AMS directions ($e > 45°$). The remaining sites, DM1 and DM3, have relatively high mean magnetic susceptibility magnitudes. Combined analysis of magnetic lineation at sites DM1 and DM3 is oriented approximately NW-SE (145N; Figure 4 and Table 1). The Didim Domain is almost undeformed but slightly tilted to south in places. However, there are some normal faults developed at the northern margin of the domain, and the mean lineation direction is perpendicular to the normal faults around the domain (Figures 5 and 6).

3.2.6. Dinar Domain

The Dinar Domain is in the northeastern part of the study area (Figure 1). It is dominated by the NW-SE striking seismically active Dinar fault and NE-SW striking normal faults controlling the domain in the east and the west (Baklan Graben; Figure 1b). The domain consist of only two sites, and both comprise Pliocene mudstones and marls. The mean magnetic susceptibility in both sites is low to moderate, ranging between 50 and 620 × 10^{-6} (SI; Table 1). The results show moderate to well scattering, and both sites have very low confidence intervals ($e < 45°$); however, they are low inclination values (BU4 = 21.3° and SK10 = 6.8°) of k_3 after tilt correction (Figure 4 and Table 1) possibly due to compaction related inclination shallowing. Combined analysis of the two sites in the domain indicate that the mean magnetic lineation is oriented 295N after tilt correction (Figure 4 and Table 1). This direction is parallel to one of the dominant normal fault sets in the domain (Figures 5 and 6).

3.2.7. Elmalı Domain

The Elmalı Domain comprises lower to middle Miocene marine turbidites in an eastward thinning sedimentary wedge, marls and limestones in the east and north. These sedimentary rocks were deposited in the Lycian

Foreland Basin (Şiş et al., 2020) developed in front of the SE verging Lycian nappes. The post middle Miocene sedimentary rocks in the domain correspond to the outer part of the foreland basin where extensional deformation is due to flexural bending of the down-going block (Beydağları Platform, Figure 1) by the load of the advancing nappes (Hayward, 1984; Şiş et al., 2020).

The Elmalı Domain was sampled at 11 sites comprising lower-middle Miocene fine sandstones-mudstone-marl and limestone rocks. Two mudstone-marl sites (EL1 and SK4) yielded erratic directions ($e > 45°$), and almost zero mean magnetic susceptibility (0×10^{-6} to -4×10^{-6} (SI) likely due to diamagnetic mineral content in the matrix, hence these sites are rejected (Table 1). Despite high magnetic susceptibility intensity (440×10^{-6} SI), site ST6 presents a triaxial cluster and mean k_3 direction that is not normal to the bedding plane (38.3°), possibly due to remagnetization (Şiş et al., 2020). In the other nine sites, the k_m values range between 44×10^{-6} and $1{,}020 \times 10^{-6}$ (SI). Sites ST1, GM are sampled in sandstone-mudstone alternations. Although the bedding attitudes vary widely from each location in the domain, the lineations are generally almost parallel to bedding strikes for each site except for site SK3 (Table 1). NW-SE striking normal faults and NE-SW striking thrust faults dominate the domain. The magnetic lineations are sub-perpendicular to the bedding strikes and clearly show two directions. Strikes at sites EL2, ST2, and ST5 are oriented NE-SW, while the remaining sites are oriented NW-SE (Figure 3 and Table 1). Combined analysis of eight sites (458 specimens) provides mean magnetic lineation of NW-SE (319N *in situ*, 142N after tilt correction) direction, which is an almost parallel to trends of the main normal fault strikes in the domain (Figures 5 and 6).

3.2.8. Fethiye Domain

The Fethiye Domain is delimited by NE-SW and NW-SE striking normal faults, which are developed under the control of multi-directional extension dominated in the WNW-ESE direction (Tosun et al., 2021). The domain is sampled by six middle Miocene to Pliocene sites composed of sandstone, mudstone, and marls. All sampled rocks show moderate to high magnetic intensity, especially the marly samples of site SK2, which reach up to $3{,}690 \times 10^{-6}$ (SI; Table 1). Thermomagnetic experiments show that ferrimagnetic (Ti-magnetite) is the dominant mineral (Figure 2). Site FE6 shows scattered AMS directions (e_1, $e_2 > 45°$) so is rejected from the interpretation. Except for site FE2, magnetic lineations are almost perpendicular to bedding strikes. The middle Miocene and Pliocene rocks are classified into two temporal groups to reconstruct mean AMS directions for each age group for the domain. The Pliocene data indicate an almost E-W magnetic lineation (082N *in situ* and 062N after tilt correction), and middle Miocene sites indicate almost a N-S (359N *in situ* and 178N after tilt correction) orientation (Table 1).

The Fethiye Domain is dominated by many normal faults developed due to ongoing extension in the region (ten Veen, 2004). Length weighted rose diagrams of the normal faults in the domain indicate two orthogonal sets of dominant fault sets striking NE-SW and NW-SE directions (Figure 6). Although the lineations from middle Miocene rocks are oblique to the any of the two dominant orthogonal normal fault sets, however, Pliocene lineations are almost parallel to NE-SW striking normal fault set, indicating NE-SW directed extension in the domain during Pliocene.

3.2.9. Ören Domain

The Ören domain is characterized by roughly E-W striking normal faults, which controlled the deposition of lower Miocene strata (Gürer and Yılmaz, 2002). From the Ören Domain, nine sites in lower to middle Miocene rocks composed of mudstone, sandstone, and marls were sampled. Among these, two sites (OR3 and YT3) were rejected because they did not result in any reliable directions and are scattered ($e > 45°$; Table 1). In addition, the YT1 and YT2 sites did not have a sufficient number of measurements for Jelinek statistics due to unconsolidated material broken into pieces during the transport. Sites OR2 and OR4 have very low to negative mean magnetic susceptibility (-2.4×10^{-6} to -5.7×10^{-6} (SI) due to diamagnetic mineral content in the matrix, and hence these sites are rejected. Despite small confidence ellipses in all three axes, site OR5 show a triaxial cluster, possibly due to intense deformation and shearing due to simple shear mechanism which destroys original stress and strain axes. Therefore, the site is rejected from the database.

The remaining two sites yielded reliable results. The magnetic lineations obtained from these sites (OR1 and OR6) are perpendicular to the local bedding strikes (Figure 4). A combination of the two sites (21 specimens) shows that the mean magnetic lineation is oriented in NW-SE (154NE before and after tilt correction, Table 1) direction, which is oblique to the NW-SE striking normal faults in the domain (Figures 5 and 6) implying possible WNW-ESE directed sinistral strike-slip shear in the domain.

3.2.10. Tavas Domain

The Tavas Domain is characterized by NE-SW striking normal faults in the eastern part and NW-SE striking normal faults, with a graben morphology in the western part. The domain developed under the influence of tectonic conditions similar to those of the Denizli Basin (Kaymakcı, 2006) and has been subjected to multi-directional extension.

The domain contains 11 sites sampled in Oligocene to upper Miocene sandstone-mudstone alternations and limestones. Site TVS4 has negative (diamagnetic) mean magnetic susceptibility -2.9×10^{-6} (SI), and maximum susceptibility directions are clustered nearly perpendicular to the bedding plane (Table 1), while sites TVS1, TVS3, TVS5, KL2, KL5, and KL6 have very large confidence ellipse ($e > 45°$). Therefore, these sites are rejected for further analysis (Table 1). The remaining four sites show very consistent results with a slight discrepancy between the lineations before and after tilt correction (Table 1). The lineations in the tilted sites are generally sub-parallel to the bedding strikes except for site TVS2, where the magnetic lineation is perpendicular to the local bedding strike (Table 1).

The sites in the Tavas Domain are grouped into two as Oligocene to middle Miocene sites (KL1–KL3 and KL4) and a site in upper Miocene rocks (TVS2). The combined analysis of Oligo-Miocene sites indicates that the mean magnetic lineation is oriented almost N-S after tilt correction (123N *in situ* and 172N after tilt correction). However, the mean magnetic lineation for the upper Miocene strata oriented almost E-W (287N *in situ* and 107N after tilt correction; Table 1).

The length weighted rose diagrams of normal faults developed in the domain indicate that two orthogonal dominant sets of normal faults are developed (Figure 6). The magnetic lineations from the Oligocene to middle Miocene rocks are oblique to any of these dominant sets, however, upper Miocene rocks are oriented parallel to almost NW-SE striking set of faults indicating NW-SE directed extension in the domain since the upper Miocene (Figure 6).

3.2.11. Ulubey Domain

The Ulubey Domain is delimited in the east by NE-SW striking normal faults that control Baklan Graben (Figure 1) and in the south by the northern boundary faults of the Denizli basin. The domain is characterized by an almost undeformed flat-lying plateau possibly influenced by tectonic conditions that gave way to the development of Baklan and Denizli basins (Figure 1).

The domain was sampled at nine sites in Pliocene limestones, sandstone, mudstone, and marl rocks cropping out in the northernmost part of the study area (Figure 1). Among these sites, five of them were rejected because they yielded very erratic directions, with poorly clustered directions ($e > 45°$), negative mean magnetic susceptibility values, and one site (UL5) presents a triaxial cluster before and after tilt correction (Table 1). The remaining four sites have moderate to high magnetic susceptibility values, and in one site, k_m reaches up to $2{,}200 \times 10^{-6}$ (SI), implying a ferrimagnetic mineral dominant composition, which is also evident from the thermomagnetic curves (Figure 2).

Among the accepted four sites, three of the magnetic lineations are oriented NE-SW, while only the UL6 is oriented NW-SE. Combined analysis of all sites indicates NNE-SSW (198N *in situ* and 200N after tilt correction) orientation of the mean magnetic lineation (k_1).

Most of the sites are undeformed, and no major tectonic activity could be observed in the Ulubey Domain. However, the southern and eastern margin of the domain is delimited by normal faults of the Denizli and Baklan grabens, the eastern continuation of the Büyük Menderes Graben (Figure 1). Length weighted rose diagrams prepared from the faults in the domain indicate that they are oriented dominantly NW-SE (Figure 6). The mean magnetic lineation direction is almost perpendicular to the NW-SE striking normal faults (dominant fault set) in the domain (Figure 6 and Table 1).

4. Discussion

4.1. Origin of Anisotropy of Magnetic Susceptibility Fabrics

The mean magnetic susceptibility axes results before and after tilt correction of 83 sites, and their domain means based on accepted (48/83) sites with the magnetic anisotropy results (L, F, P_j, T, etc.) are listed in Table 1. The results per site are shown in Figure 4. To illustrate an approximate qualitative magnetic mineralogy of all analyzed sites, we plot the mean susceptibility values (k_m) of all specimens from both Oligocene-Miocene and upper Miocene to Pliocene sedimentary rocks (Figure 6). The k_m values show a wide range, from very low values around 0×10^{-6} SI up to very high values of more than $6{,}000 \times 10^{-6}$ SI. There are two main mean frequencies, one around $25–75 \times 10^{-6}$ (mostly upper Miocene to Pliocene rocks) and one around $1{,}000 \times 10^{-6}–5{,}000 \times 10^{-6}$ SI (mostly Oligocene - middle Miocene rocks; Figure 3 and Table 1). When the Miocene and Pliocene samples are compared, the Miocene specimens exhibit the highest susceptibilities and dominate the high susceptibility cluster, consistent with their rock type, as fine detrital mudstones and marls. In contrast, samples of rocks of upper Miocene to Pliocene were collected dominantly from sandstones and claystones (Figure 3d). The k_m values show a wide range proving that the specimens include a varying composition and concentration of (ferri-) magnetic minerals. In addition, the k_m distribution seems to be partly dependent on the age of the specimens because lower-middle Miocene samples tend to have larger values. Distributions of the maximum (k_1), intermediate (k_2), and minimum (k_3) susceptibility axes at the site level exhibit a variable degree of clustering from quite scattered (large confidence ellipses; $e > 45°$) to very well-defined clusters (Table 1). As above, the sites with statistically insufficient samples and that show considerable scatter in the three susceptibility axes (confidence ellipses >45°) were excluded from further analysis. The rejected site mean results are given in Table 1, and accepted sites are shown in Figure 4. Most of the rejected sites (35 in total) have very low to negative susceptibilities (diamagnetic) and those data cannot be interpreted.

The distribution of the susceptibility axes directions after tilt correction from the remaining accepted (48) sites generally presents a predominantly oblate shape, reflecting the essentially sedimentary origin of the fabric (k_3 typically perpendicular to the bedding plane). However, the clustering of the k_1 and k_2 axes reflects the type and magnitude of the tectonic deformation prevailing in the region. The mean foliation parameters (F) have small scattering ranging $1.003 \leq F \leq 1.078$ ($F_{mean} = 1.025$). Site mean magnetic lineation (L) parameters range $1.002 \leq L \leq 1.033$ ($L_{mean} = 1.008$). F_{mean} is slightly higher than L_{mean}—it is clear from Figure 3c that most of the foliation values are higher than the lineation values, reflecting the mainly oblate character of the distributions, in particular for the range with both L and F <1.2. The corrected anisotropy degree P_j is, in general, relatively low with a dominant mean clustering around $P_j = 1.02$. In general, the shape of the AMS ellipsoids is mostly moderately oblate (Figure 3c), but also negative T values (prolate) occur. We note that there is no evident correlation between T and P_j, indicating that the lithologic and spatio-temporal distribution of the sites is almost equally affected by tectonic deformation. This implies that the observed AMS fabrics formed in response to tectonism or a combination of sedimentary and tectonic processes (Figures 3c and 3d).

4.2. Interpretation of Results

In addition to the spatial differences in orientations of susceptibility axes, variations in magnitude of magnetic susceptibility show that some bulk magnetic susceptibilities are clustered as low as around 50×10^{-6} SI, whereas others cluster as high as around $5{,}000 \times 10^{-6}$ SI (Figure 3). The low and high values are interpreted to be associated with the dominances of diamagnetic/paramagnetic or ferrimagnetic minerals in the samples, respectively (Figure 3a). According to previous studies, the dominance of either paramagnetic and ferrimagnetic minerals in a rock volume does not affect the AMS patterns (e.g., Borradaile & Jackson, 2010). Paramagnetic phyllosilicate (e.g., clay) minerals are highly sensitive in terms of strain indicators, more than classical strain analyses methods in weakly deformed areas (Scheepers & Langereis, 1994).

In ideal conditions, such as a low energy, vertical (no flow involved) depositional environment, the presence of suitable magnetic minerals in the absence of diagenetic or other post-depositional petrologic changes, the maximum anisotropy axis (k_1) aligns parallel to the maximum stretching direction in extensional settings. On the other hand, k_1 is aligned parallel to σ_2 in the compressional-contractional settings (Qayyum et al., 2021). In both cases, pure shear conditions must have prevailed in the region (e.g., Gong et al., 2009; Maffione et al., 2015; Mattei et al., 1997; Scheepers & Langereis, 1994; Soto et al., 2009). In this study, the magnetic fabric orientations in

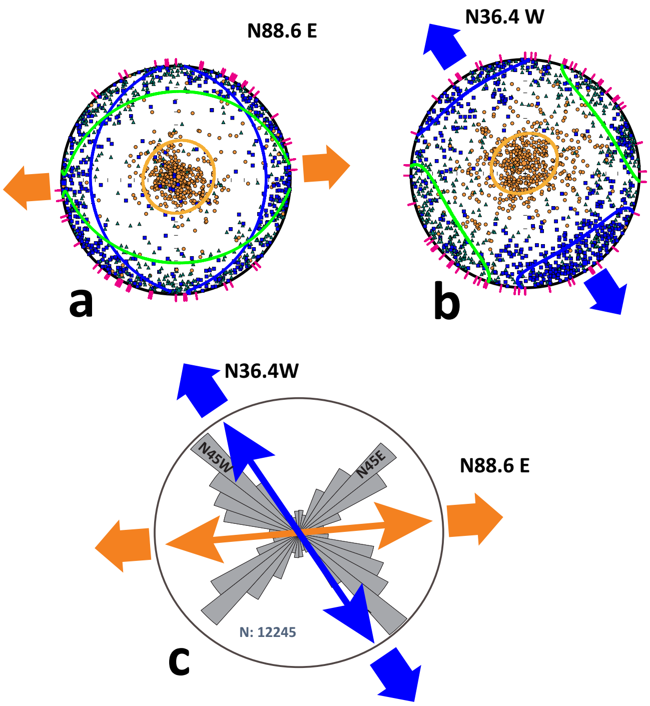

Figure 7. Lower hemisphere equal area plots of AMS axes for rocks of (a) Oligocene to middle Miocene (arrows in orange color) and (b) late Miocene to Pliocene age (arrows in blue color). (c) Rose diagrams of all the fault strikes in the study area and dominant orientations of AMS lineations.

the Neogene sedimentary rocks are from one of the most tectonically active extensional deformation dominated regions in the eastern Mediterranean and are used to decipher past and recent deformation patterns. The AMS tensor provides information about the geometry of the strain ellipsoid (e.g., Cifelli et al., 2004, 2005). The AMS shape parameter (T) versus corrected anisotropy degree (P_j) diagram (Figure 6c) indicate that most of the measurements yield positive T values (clustered in the oblate region) and suggest a considerable amount of compaction (e.g., Tarling & Hrouda, 1993). However, the systematic clustering of maximum (k_1) and intermediate (k_2) anisotropy axes in the horizontal plane suggests that the sedimentary fabric has been modified into a tectono-sedimentary fabric that facilitates determination and quantification of strain axes in space and time.

The AMS data from Oligocene to Pliocene sedimentary sequences from the entire SW Anatolia (from 83 sites in 11 domains) are documented in this study. Except for sites with diamagnetic susceptibilities and/or scattered distributions, the AMS results show that the magnetic fabrics of the detrital sedimentary rocks result from tectonic deformation. These deformation-related AMS patterns are characterized by an orientation parallel or perpendicular to the bedding strikes and a well-defined magnetic lineation with low error ellipsoids (Figure 3 and Table 1). The results show that the magnetic fabrics of the sites that we have accepted from Neogene deposits indicate an apparent tectonic overprint (Table 1).

The study area is dominated by two families of structures, oriented in NE-SW and NW-SE directions (Figures 4 and 7). They are developed under multi-directional extension with triaxial strain conditions (cf. Kaymakcı, 2006; Krantz, 1988; Reches, 1978). Therefore, the main magnetic lineations at specific sites are either parallel or almost perpendicular to one of the sets of adjacent faults. On the other hand, almost all of the Oligocene to middle Miocene rocks in the Tavas, Ören, and Fethiye basins yield oblique lineations to the adjacent local major normal faults. The results also indicate that bedding strikes and maximum anisotropy directions are almost perpendicular to each other, except for a few sites, mainly in the Fethiye and Elmalı domains, where compressional deformation prevailed during the early to middle Miocene. Considering the late Miocene to Recent extensional regime in the region, it is safe to assume that tilting of strata is the result of normal faulting, therefore the strikes of the faults and bedding are almost parallel to each other, which are also mostly perpendicular to the mean magnetic lineations.

In order to obtain mean magnetic lineation directions for each domain, the results are categorized based on the rock ages. The results yielded 13 mean AMS directions for 11 domains (Figure 5 and Table 1). These are produced by grouping data from the Oligocene to middle Miocene and upper Miocene to Pliocene sequences separately. Obtained mean directions are compared with the length weighted rose diagrams of the normal fault trends in each domain (Figure 6). The unit length of each fault is taken as 250 m. As seen in Figure 6, except Dinar domain, in all other domains show that mean AMS directions are almost parallel to one of the dominant sets of the normal faults. The directions, which are essentially perpendicular to the most dominant set, are interpretable because they indicate major extension directions during and after sedimentation, as the main basin bounding normal faults are perpendicular to the extension directions.

In Figure 7, AMS ellipsoids based on the age and shape factor (T in Table 1) are given. Pre-upper Miocene rocks (Figure 7a) in the Ören, Elmalı, Tavas, and Fethiye yield prolate magnetic fabric indicating almost E-W oriented extension. On the other hand, combined analysis of the AMS data from all upper Miocene to Pliocene sites indicate almost NW-SE directed extension, although individual orientations are scattered almost radially (Figure 7b). Similarly, the length weighted rose diagram prepared from the strikes of the faults developed in the study area (Figure 7c) indicates that the faults in SW Anatolia can be grouped into two orthogonal sets oriented in NE-SW and NW-SE directions. The late-Miocene to Pliocene magnetic lineations are almost parallel to the NW-SE striking fault set, however, Oligocene to middle Miocene magnetic lineations are not parallel to any of the orthogonal fault set and they are oblique to both of them.

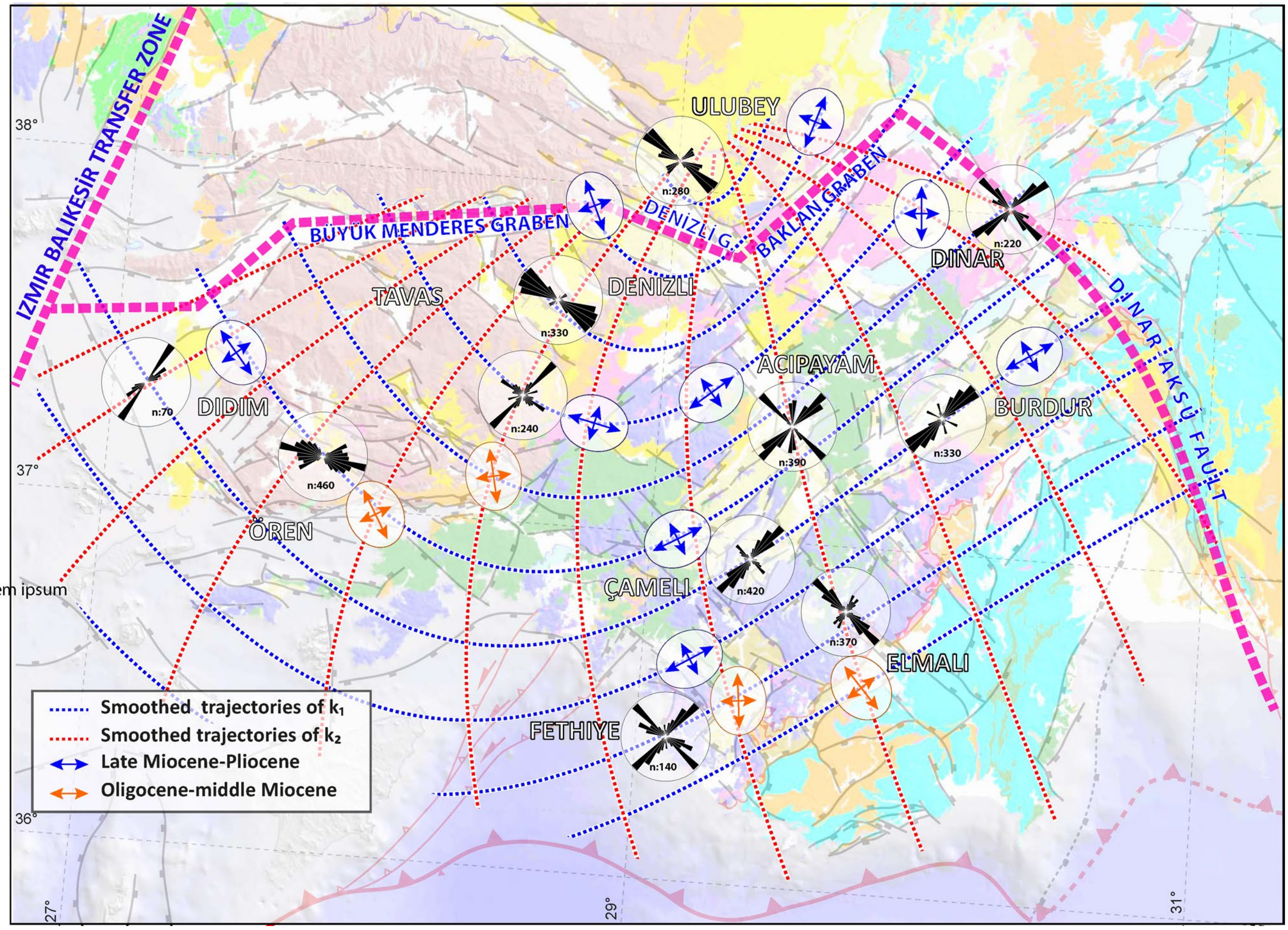

Figure 8. Strain ellipses based on directions of k_1 and k_2 and rose diagrams of the fault strikes and for each structural domain. *Note*. Isotropic point around Ulubey domain.

Using the general trends of the magnetic lineations (k_1 and k_2), smoothed trajectories are constructed manually for the late Miocene to Pliocene time interval (Figure 8). The mean magnetic lineations, hence maximum extension directions for almost all domains are parallel to the smoothed trajectories except for Dinar domain (Figure 8). In addition, all of the Oligocene to middle Miocene magnetic directions are oblique to the constructed trajectories. This relation can be explained by block rotations that affected the region (Kaymakcı et al., 2018).

4.3. Regional Implications

The combined analysis of the results indicates two spatiotemporally distinct directions, although individual sites and domains vary considerably. The domains exposing Oligocene to middle Miocene rocks indicate approximately E-W oriented extension, and late Miocene to Pliocene domains indicate NW-SE oriented extension (Figure 7), which are almost perpendicular to each other. This relationship implies that the dominant extension direction has changed in the region from E-W to NW-SE by the end of the middle Miocene. However, recent field data (Kaymakcı, 2006), moment tensor solutions (Shah, 2015; Tan et al., 2008), and GPS vectors (Elitez et al., 2016) indicate that the region was under the influence of multi-directional extension until recently. Nevertheless, E-W and NW-SE oriented least principal stress (σ_3) slightly dominate over other directions within almost vertical uniaxial stress conditions.

The Miocene exhumation of metamorphic core complexes in the region is associated with the extensional deformation resulting from the southward retreat of the northwards subducted African slab below the western Anatolian and Aegean regions (Gessner et al., 2013; Kaymakcı et al., 2018; Uzel et al., 2015). These processes are associated with the exhumation of the Cycladic Complex in the south. The extensional strain between

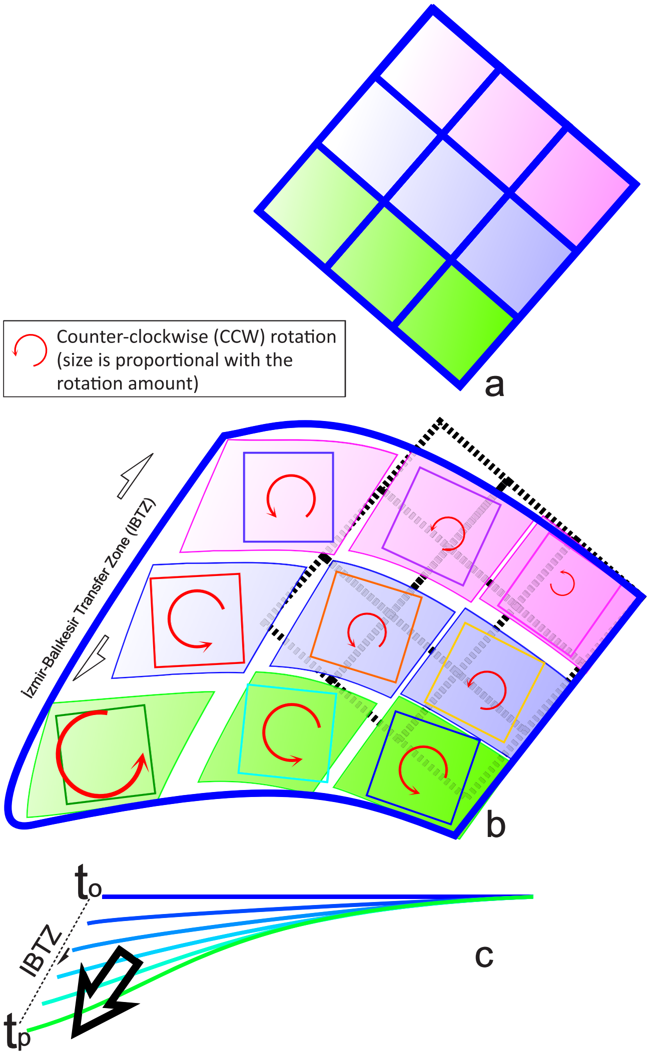

Figure 9. Schematic representation of SW-directed Stretching rubber sheet deformation model and associated counterclockwise rotation proposed for SW Anatolia. (a) Original geometry, (b) deformed geometry, and (c) position of a starting E-W imaginary line from Oligocene (t_0) to present (t_p). Large black arrow shows the main stretching direction. The NE corner of the model approximately corresponds to the Burdur domain. *Note*. The change in the shapes of originally square blocks. Rotation senses and magnitudes, and the rubber sheet model is adopted from Kaymakcı et al. (2018).

these complexes is partitioned with the development of a crustal-scale İzmir-Balıkesir Transfer Zone (İBTZ) dominated by transtensional deformation (Uzel et al., 2013, 2015; Westerweel et al., 2020). On the eastern side of the Menderes Core Complex, a similar transtensional shear zone, namely Fethiye-Burdur Shear Zone (Hall et al., 2014) has also been proposed. However, some authors criticized the presence of such a sinistral shear zone (e.g., Alçiçek, 2015; Kaymakcı et al., 2018; Özkaptan et al., 2018) and argued that such a shear zone would produce strike-slip kinematic indicators, although documented structural features are mainly related to normal faulting along the proposed zone (Özkaptan et al., 2018), unlikely the İBTZ (e.g., Uzel et al., 2013, 2015; Westerweel et al., 2020). Besides, a very prominent differential rotation of fault blocks within and outside of such a shear zone would have been developed (Kaymakcı et al., 2018).

The AMS results presented here indicate smooth transitions of the principal strain axes across the region, which is not consistent with the presence of a NE-SW oriented strike-slip shear zone extending from Fethiye to Burdur domains as was previously argued (Kaymakcı et al., 2018, Özkaptan et al., 2018; Tosun et al., 2021).

Paleomagnetic studies carried out on the same Neogene sedimentary sequences in the region (Alçiçek et al., 2016; Gürsoy et al., 2003; Kaymakcı et al., 2018; Kissel & Laj, 1988; Koç et al., 2016; Özkaptan et al., 2014; Tatar et al., 2002; Uzel et al., 2015), as well as a few magnetostratigraphic studies (Özkaptan et al., 2018; Şen & Seyitoğlu, 2009) and the studies based on fault kinematics, seismotectonic and Global Navigation Satellite System based active deformation studies in the region, all indicate multi-directional extension (Aktuğ et al., 2009; Alçiçek, 2007; Alçiçek et al., 2005, 2006, 2012, 2013, 2018; Barka & Reilinger, 1997; Kaymakcı et al., 2018; Price & Scott, 1994; Taymaz & Price, 1992; ten Veen et al., 2009).

There is a major change in the orientation of the magnetic lineations from sites to the north and the south of the major domain boundary, that is, approximately defined by Büyük Menderes-Denizli-Baklan grabens in the west and Dinar-Aksu faults (Kaymakcı et al., 2018) in the east (Figure 8). This boundary also marks the boundary between clockwise and counterclockwise rotating regions in western Anatolia (Kaymakcı et al., 2018). To this end, we propose that differential extension and rotational deformation in the region gave way to the development of small checkerboard-like pattern of fault blocks south of this line, their rotation and translation of which has produced complex deformation and even locally contrasting deformation styles in the region. Rotation and non-rigid deformation resulted in both inhomogeneous strain and the development of discrete shear (transfer) zones between these blocks that have been shaping the deformation style and tectonic pattern in the region since the early Miocene (Kaymakcı et al., 2018).

Our new AMS results reveal the tectonic style and amount of crustal deformation in SW-Anatolia. The variations in the deformation axes gradually change between the domains, while the strain ellipsoid shape factor is almost the same for all the upper Miocene to Pliocene sedimentary sequences. Based on these results and the literature (e.g., Kaymakcı et al., 2018 and references therein), we conclude that SW Anatolia experienced multi-directional extension associated with counterclockwise rotation exerted by the southward retreat of the Eastern Mediterranean subduction system and this deformation continues today. This resulted in stretching of the SW Anatolia, the over-riding plate, to accommodate the retreat of the trench by a non-rigid stretched rubber-sheet like deformation style (Figure 9), which seems to be pulled from a single point in a SW direction (Kaymakcı et al., 2018). The Büyük Menderes-Denizli-Baklan grabens and Dinar-Aksu faults mark the northern boundary of this peculiar deformation zone.

5. Conclusions

The tectono-sedimentary magnetic fabrics in the rocks of Oligocene-Pliocene basins in SW Anatolia suggest that the original sedimentary (purely compactional) fabrics of these sedimentary rocks have been overprinted by increasing strain effects closely linked to the Cenozoic tectonism.

The distinct AMS patterns result from tectonic deformation; hence they are parallel to the principal strain axes, such that k_1 corresponds to major extension direction, and k_3, which is almost normal to the bedding, correspond to sedimentary compaction.

Anisotropy of magnetic susceptibility (AMS) results from weakly deformed Oligocene to Pliocene sedimentary rocks from 83 sites dispersed over entire SW Anatolia reveal two dominant extension directions. These are E-W for Oligocene to middle Miocene and NW-SE for late Miocene to Pliocene.

The major extension directions, both on a within-site basis and a combined analysis of the sites into deformation domains, are generally parallel or perpendicular to the major faults in each domain and bedding strikes.

Deformation in SW Anatolia is characterized by multi-directional extension with the dominance of E-W and NW-SE orientations associated with the southward retreat of the trench related to the eastern Mediterranean subduction system, which resulted in the SW stretched rubber sheet-like deformation of SW Anatolia.

The results reported do not support the presence of a major sinistral shear zone within the region.

Data Availability Statement

The paleomagnetic anisotropy of magnetic susceptibility data obtained in this study is measured and analyzed using AGICO-Anisoft v.4.2 Anisotropy data software. The output data is stored in EarthRef.org database can be downloaded from: http://earthref.org/ERDA/download:2503/.

Acknowledgments

This study was supported by the Scientific and Technical Research Council of Turkey (TÜBİTAK) Grant Number ÇAYDAG-111Y239. We would like to thank Pınar Ertepınar, Ayten Koç, and Côme Lefebvre for their support during sample collection in the field. We also thank John Geissman and an anonymous reviewer for their positive suggestions and improving the English of the article. All the data presented here are completely new, and we have not used any anisotropy of magnetic susceptibility data from the literature nor any repositories.

References

Aktuğ, B., Nocquet, J. M., Cingöz, A., Parsons, B., Erkan, Y., England, P., et al. (2009). Deformation of western Turkey from a combination of permanent and campaign GPS data: Limits to block-like behavior. *Journal of Geophysical Research*, *114*(B10). https://doi.org/10.1029/2008JB006000

Alçiçek, M. C. (2007). Tectonic development of an orogen-top rift recorded by its terrestrial sedimentation pattern: The Neogene Eşen Basin of southwestern Anatolia, Turkey. *Sedimentary Geology*, *200*(1–2), 117–140. https://doi.org/10.1016/j.sedgeo.2007.04.003

Alçiçek, M. C. (2015). Comment on 'The Fethiye-Burdur Fault Zone: A component of upper plate extension of the Subduction Transform Edge Propagator fault linking Hellenic and Cyprus Arcs, Eastern Mediterranean. Tectonophysics, 635, 80–99' by J. Hall, A.E. Aksu, I. Elitez, C. Yaltırak. *Tectonophysics*, *664*, 1–4. https://doi.org/10.1016/j.tecto.2015.01.025

Alçiçek, M. C., Brogi, A., Capezzuoli, E., Liotta, D., & Meccheri, M. (2013). Superimposed basin formation during Neogene-Quaternary extensional tectonics in SW-Anatolia (Turkey): Insights from the kinematics of the Dinar Fault Zone. *Tectonophysics*, *608*, 713–727. https://doi.org/10.1016/j.tecto.2013.08.008

Alçiçek, M. C., Kazanci, N., & Özkul, M. (2005). Multiple rifting pulses and sedimentation patterns in the Çameli Basin, southwestern Anatolia, Turkey. *Sedimentary Geology*, *173*, 409–431.

Alçiçek, M. C., Mayda, S., & Alçiçek, H. (2012). Faunal and palaeoenvironmental changes in the çal Basin, SW Anatolia: Implications for regional stratigraphic correlation of late Cenozoic basins. *Comptes Rendus Geoscience*, *344*(2), 89–98. https://doi.org/10.1016/j.crte.2012.01.003

Alçiçek, M. C., Mayda, S., & Arzu Demirel, F. (2016). Discussion on "Neogene-Quaternary evolution of the Tefenni basin on the Fethiye-Burdur fault zone, SW Anatolia-Turkey. Journal of African Earth Sciences, 118, 137–148" by R. Aksoy, S. Aksarı. *Journal of African Earth Sciences*. https://doi.org/10.1016/j.jafrearsci.2016.07.024

Alçiçek, M. C., Mayda, S., ten Veen, J. H., Boulton, S. J., Neubauer, T. A., Alçiçek, H., et al. (2019). Reconciling the stratigraphy and depositional history of the Lycian orogen-top basins, SW Anatolia. *Palaeobiodiversity and Palaeoenvironments*, *99*(4), 551–570. https://doi.org/10.1007/s12549-019-00394-3

Alçiçek, M. C., ten Veen, J. H., & Özkul, M. (2006). Neotectonic development of the Çameli Basin, southwestern Anatolia, Turkey. In A. H. F. Robertson & D. Mountrakis (Eds.), *Tectonic development of the eastern Mediterranean region* (Vol. 260, pp. 591–611). Geological Society, London, Special Publications.

Alçiçek, M. C., van den Hoek Ostende, L. W., Saraç, G., Tesakov, A. S., Murray, A. M., Hakyemez, H. Y., et al. (2018). Comment on "Miocene to Quaternary tectonostratigraphic evolution of the middle section of the Burdur-Fethiye Shear Zone, south-western Turkey: Implications for the wide inter-plate shear zones. *Tectonophysics* 690, 336–354". *Tectonophysics*, *722*, 595–600. https://doi.org/10.1016/J.TECTO.2017.05.027

Barka, A. A., & Reilinger, R. (1997). Active tectonics of the Eastern Mediterranean Region: Deduced from GPS, neotectonic and seismic data. *Annali di Geofisica*, *40*(3), 587–610. https://doi.org/10.1111/j.1365-2486.2011.02460.x

Biryol, C., Beck, S. L., Zandt, G., & Özacar, A. A. (2011). Segmented African lithosphere beneath the Anatolian region inferred from teleseismic P-wave tomography. *Geophysical Journal International*, *184*(3), 1037–1057. https://doi.org/10.1111/j.1365-246X.2010.04910.x

Borradaile, G. J. (1988). Magnetic susceptibility, petrofabrics, and strain. *Tectonophysics*, *156*, 1–20. https://doi.org/10.1016/0040-1951(88)90279-X

Borradaile, G. J. (1991). Correlation of strain with anisotropy of magnetic susceptibility (AMS). *Pure and Applied Geophysics*, *135*(1), 15–29. https://doi.org/10.1007/BF00877006

Borradaile, G. J., & Henry, B. (1997). Tectonic applications of magnetic susceptibility and its anisotropy. *Earth-Science Reviews*, *42*(1–2), 49–93. https://doi.org/10.1016/S0012-8252(96)00044-X

Borradaile, G. J., & Jackson, M. (2010). Structural geology, petrofabrics, and magnetic fabrics (AMS, AARM, AIRM). *Journal of Structural Geology*, *32*, 1519–1551. https://doi.org/10.1016/j.jsg.2009.09.006

Chadima, M., & Jelinek, V. (2009). *Anisoft 4.2: Anisotropy data browser for windows*. AGICO, Inc.

Cifelli, F., Mattei, M., Chadima, M., Hirt, A. M., & Hansen, A. (2005). The origin of tectonic lineation in extensional basins: Combined neutron texture and magnetic analyses on 'undeformed' clays. *Earth and Planetary Science Letters*, *235*, 62–78. https://doi.org/10.1016/j.epsl.2005.02.042

Cifelli, F., Mattei, M., Hirt, A. M., & Günther, A. (2004). The origin of tectonic fabrics in 'undeformed' clays: The early stages of deformation in extensional sedimentary basins. *Geophysical Research Letters*, *31*(9). https://doi.org/10.1029/2004GL019609

Collinson, D. W. (1983). *Methods in rock magnetism and palaeomagnetism. Paleomagnetism-techniques and instrumentation*. Chapman & Hall.

Dankers, P. H. M. (1978). *Magnetic properties of dispersed natural iron-oxides of known grain-size*. (p. 143). (PhD thesis). Rijksuniversiteit te.

Duermeijer, C. E. E., van Vugt, N., Langereis, C. G. G., Meulenkamp, J. E. E., & Zachariasse, W. J. J. (1998). A major late Tortonian rotation phase in the Crotone basin using AMS as tectonic tilt correction and timing of the opening of the Tyrrhenian basin. *Tectonophysics*, *287*(1–4), 233–249. https://doi.org/10.1016/S0040-1951(98)80071-1

Elitez, İ., & Yaltırak, C. (2016). Extensional and compressional regime driven left-lateral shear in southwestern Anatolia (eastern Mediterranean): The Burdur-Fethiye Shear Zone. *Tectonophysics*, *688*, 26–35. https://doi.org/10.1016/j.tecto.2016.09.024

Elitez, İ., Yaltırak, C., & Aktuğ, B. (2016). Extensional and compressional regime driven left-lateral shear in southwestern Anatolia (eastern Mediterranean): The Burdur-Fethiye Shear Zone. *Tectonophysics*, *688*, pp.26-35.

Fabian, K., Shcherbakov, V. P., & McEnroe, S. A. (2013). Measuring the Curie temperature. *Geochemistry, Geophysics, Geosystems*, *14*(4), 947–961. https://doi.org/10.1029/2012GC004440

Faccenna, C., Bellier, O., Martinod, J., Piromallo, C., & Regard, V. (2006). Slab detachment beneath eastern Anatolia: A possible cause for the formation of the North Anatolian Fault. *Earth and Planetary Science Letters*, *242*, 85–97. https://doi.org/10.1016/j.epsl.2005.11.046

Ferré, E. C. (2002). Theoretical models of intermediate and inverse AMS fabrics. *Geophysical Research Letters*, *29*(7), 31-1–31-4.

General Directorate, MTA. (2002). *1/500k scale geological map series of Turkey*.

Gessner, K., Gallardo, L.A., Markwitz, V., Ring, U. and Thomson, S.N. (2013). What caused the denudation of the Menderes Massif: Review of crustal evolution, lithosphere structure, and dynamic topography in southwest Turkey. *Gondwana Research*, *24*(1), pp.243-274.

Gong, Z., van Hinsbergen, D. J. J., Vissers, R. L. M., & Dekkers, M. J. (2009). Early Cretaceous syn-rotational extension in the Organya basin-New constraints on the palinspastic position of Iberia during its rotation. *Tectonophysics*, *473*(3–4), 312–323. https://doi.org/10.1016/j.tecto.2009.03.003

Govers, R., & Wortel, M. J. R. (2005). Lithosphere tearing at STEP faults: Response to edges of subduction zones. *Earth and Planetary Science Letters*, *236*, 505–523. https://doi.org/10.1016/j.epsl.2005.03.022

Graham, J. (1966). Significance of magnetic anisotropy in Appalachian sedimentary rocks. In J. S Steinhart & T. J. Smith (Eds.), *The Earth beneath the continents: A volume of geophysical studies in honor of Merle A. Tuve (Geophysical Monograph Series)*, (Vol. 10, pp. 627–648). American Geophysical Union.

Gürer, Ö. F., & Yilmaz, Y. (2002). Geology of the Ören and surrounding areas, SW Anatolia. *Turkish Journal of Earth Sciences*, *11*(1), 1–13.

Gürsoy, H., Piper, J. D. A., & Tatar, O. (2003). Neotectonic deformation in the western sector of tectonic escape in Anatolia: Palaeomagnetic study of the Afyon region, central Turkey. *Tectonophysics*, *374*(1–2), 57–79. https://doi.org/10.1016/S0040-1951(03)00346-9

Hall, J., Aksu, A. E., Elitez, I., Yaltirak, C., Çifçi, G., & Yaltırak, C. (2014). The Fethiye–Burdur Fault Zone: A component of upper plate extension of the subduction transform edge propagator fault linking Hellenic and Cyprus Arcs, Eastern Mediterranean. *Tectonophysics*, *635*, 80–99. https://doi.org/10.1016/j.tecto.2014.05.002

Hayward, A. B. (1984). Sedimentation and basin formation related to ophiolite nappe emplacement, Miocene, SW Turkey. *Sedimentary Geology*, *71*, 105–129. https://doi.org/10.1016/0037-0738(84)90042-3

Hirt, A. M., Evans, K. F., & Engelder, T. (1995). Correlation between magnetic anisotropy and fabric for Devonian shales on the Appalachian Plateau. *Tectonophysics*, *247*(1–4), 121–132. https://doi.org/10.1016/0040-1951(94)00176-A

Hirt, A. M., Lowrie, W., Clendenen, W. S., & Kligfield, R. (1993). Correlation of strain and the anisotropy of magnetic susceptibility in the Onaping Formation: Evidence for a near-circular origin of the Sudbury Basin. *Tectonophysics*, *225*(4), 231–254. https://doi.org/10.1016/0040-1951(93)90300-9

Hrouda, F. (1982). Magnetic anisotropy of rocks and its application in geology and geophysics. *Geophysical surveys*, *5*(1), pp.37-82.

Hrouda, F. (1991). Models of magnetic anisotropy variations in sedimentary thrust sheets. *Tectonophysics*, *185*(3–4), 203–210. https://doi.org/10.1016/0040-1951(91)90444-W

Hrouda, F. (1993). Theoretical models of magnetic anisotropy to strain relationship revisited. *Physics of the Earth and Planetary Interiors*, *77*(3–4), 237–249. https://doi.org/10.1016/0031-9201(93)90101-E

Jelínek, V. (1977). *The statistical theory of measuring anisotropy of magnetic susceptibility of rocks and its application*. Geofyzika.

Jelínek, V. (1978). Statistical processing of magnetic susceptibility measured on groups of specimens. *Studia Geophysica et Geodaetica*, *22*, 50–62.

Jelínek, V. (1981). Characterization of the magnetic fabric of rocks. *Tectonophysics*, *79*(3–4), T63–T67. https://doi.org/10.1016/0040-1951(81)90110-4

Kaymakcı, N. (2006). Kinematic development and paleostress analysis of the Denizli Basin (Western Turkey): Implications of spatial variation of relative paleostress magnitudes and orientations. *Journal of Asian Earth Sciences*, *27*(2), 207–222. https://doi.org/10.1016/j.jseaes.2005.03.003

Kaymakcı, N., Langereis, C., Özkaptan, M., Özacar, A. A., Gülyüz, E., Uzel, B., & Sözbilir, H. (2018). Paleomagnetic evidence for upper plate response to a STEP fault, SW Anatolia. *Earth and Planetary Science Letters*, *498*, 101–115. https://doi.org/10.1016/j.epsl.2018.06.022

Kissel, C., Barrier, E., Laj, C., & Lee, T. Q. (1986). Magnetic fabric in "undeformed" marine clays from compressional zones. *Tectonics*, *5*(5), 769–781. https://doi.org/10.1029/TC005i005p00769

Kissel, C., & Laj, C. (1988). The tertiary geodynamical evolution of the Aegean arc: A paleomagnetic reconstruction. *Tectonophysics*, *146*, 183–201. https://doi.org/10.1016/0040-1951(88)90090-x

Kodama, K. P. (1995). Remanence anisotropy as a correction for inclination shallowing: A case study of the Nacimiento Formation. *Eos, Transactions of the American Geophysical Union*, *76*, 160–161.

Konak, N., & Şenel, M. (2002). *1/500.000 scale geological map of Turkey, İzmir sheet*. General Directorate of Mineral Research and Exploration (MTA).

Koç, A., van Hinsbergen, D. J. J., Kaymakcı, N., & Langereis, C. G. (2016). Late Neogene oroclinal bending in the central Taurides: A record of terminal eastward subduction in southern Turkey. *Earth and Planetary Science Letters*, *434*, 75–90. https://doi.org/10.1016/J.EPSL.2015.11.020

Krantz, R.W. (1988). Multiple fault sets and three-dimensional strain: Theory and application. *Journal of Structural Geology*, *10*(3), 225-237.

Le Pichon, X., & Angelier, J. (1979). The Hellenic arc and trench system: A key to the neotectonic evolution of the Eastern Mediterranean area. *Tectonophysics*, *60*, 1–42. https://doi.org/10.1016/0040-1951(79)90131-8

Lüneburg, C. M., Lampert, S. A., Lebit, H. D., Hirt, A. M., Casey, M., & Lowrie, W. (1999). Magneticanisotropy, rockfabrics and finite strain in deformed sediments of SW Sardinia (Italy). *Tectonophysics*, *307*, 51–74.

Maffione, M., Hernandez-Moreno, C., Ghiglione, M. C., Speranza, F., van Hinsbergen, D. J. J., & Lodolo, E. (2015). Constraints on deformation of the Southern Andes since the Cretaceous from anisotropy of magnetic susceptibility. *Tectonophysics*, *665*, 236–250. https://doi.org/10.1016/j.tecto.2015.10.008

Maffione, M., Pucci, S., Sagnotti, L., & Speranza, F. (2012). Magnetic fabric of Pleistocene continental clays from the hanging-wall of an active low-angle normal fault (Altotiberina Fault, Italy). *International Journal of Earth Sciences*, *101*(3), 849–861. https://doi.org/10.1007/s00531-011-0704-9

Mattei, M., Sagnotti, L., Faccenna, C., & Funiciello, R. (1997). Magnetic fabric of weakly deformed clay-rich sediments in the Italian peninsula: Relationship with compressional and extensional tectonics. *Tectonophysics*, *271*(1–2), 107–122. https://doi.org/10.1016/S0040-1951(96)00244-2

Mattei, M., Speranza, F., Argentieri, A., Rosetti, F., Sagnotti, L., & Funiciello, R.(1999). Extensional tectonics in the Amantea basin (Calabria, Italy): A comparison between structural and magnetic anisotropy data. *Tectonophysics*, *307*(1-2), 33–49.

Mullender, T. A. T., Van Velzen, A. J., & Dekkers, M. J. (1993). Continuous drift correction and separate identification of ferrimagnetic and paramagnetic contribution in thermamagnetic runs. *Geophysical Journal International*, *114*, 663–672. https://doi.org/10.1111/j.1365-246x.1993.tb06995.x

Noltimier, H. C. (1971). Magnetic rock cylinders with negligible shape anisotropy. *Journal of Geophysical Research*, *76*(17), 4035–4037. https://doi.org/10.1029/jb076i017p04035

Oliva-Urcia, B., Rahl, J. M., Schleicher, A. M., & Pares, J. M. (2010). Correlation between the anisotropy of the magnetic susceptibility, strain and X-ray texture goniometry in phyllites from Crete, Greece. *Tectonophysics*, *486*, 120–131. https://doi.org/10.1016/j.tecto.2010.02.013

Özkaptan, M., & Gülyüz, E. (2019). Relationship between the anisotropy of magnetic susceptibility and development of the Haymana Anticline, Central Anatolia (Turkey). *Turkish Journal of Earth Sciences*, *28*(1), 103–121.

Özkaptan, M., Kaymakcı, N., Langereis, C. G., Gülyüz, E., Arda Özacar, A., Uzel, B., & Sözbilir, H. (2018). Age and kinematics of the Burdur Basin: Inferences for the existence of the Fethiye Burdur Fault Zone in SW Anatolia (Turkey). *Tectonophysics*, *744*, 256–274. https://doi.org/10.1016/j.tecto.2018.07.009

Özkaptan, M., Koç, A., Lefebvre, C., Gülyüz, E., Uzel, B., Kaymakcı, N., et al. (2014). Kinematics of SW Anatolia implications on crustal deformation above slab tear. *Geophysical Research Abstracts*, *16*, EGU2014-6061-1.

Parés, J. M., & van der Pluijm, B. A. (2002). Phyllosilicate fabric characterization by low-temperature anisotropy of magnetic susceptibility (LT-AMS). *Geophysical Research Letters*, *29*(24), 68-1–68-4. https://doi.org/10.1029/2002GL015459

Parés, J.M. & Van der Pluijm, B.A. (2004). Correlating magnetic fabrics with finite strain: Comparing results from mudrocks in the Variscan and Appalachian Orogens. *Geologica Acta: an international earth science journal*, *2*(3), pp.213-220.

Parés, J. M., Van der Pluijm, B. A., & Dinarès-Turell, J. (1999). Evolution of magnetic fabrics during incipient deformation of mudrocks (Pyrenees, northern Spain). *Tectonophysics*, *307*(1–2), 1–14. https://doi.org/10.1016/S0040-1951(99)00115-8

Passier, H. F., De Lange, G. J., & Dekkers, M. J. (2001). Magnetic properties and geochemistry of the active oxidation front and the youngest sapropel in the eastern Mediterranean sea. *Geophysical Journal International*, *145*(3), 604–614. https://doi.org/10.1046/j.0956-540X.2001.01394.x

Price, S. P., & Scott, B. C. (1994). Fault-block rotations at the edge of a zone of continental extension, southwest Turkey. *Journal of Structural Geology*, *16*, 381–392. https://doi.org/10.1016/0191-8141(94)90042-6

Qayyum, A., Poessé, J. W., Nuretdin Kaymakcı, C. G., Langereis, E. G., & Ahsan, N. (2021). Neogene kinematics of the Potwar plateau and the Salt range, NW Himalayan front: A paleostress inversion and AMS study. *International Geology Review*.

Ramsey, J. G., & Huber, M. I. (1983). Instructor's manual to accompany the techniques of modern structural geology. *Strain analysis* (Vol. 1). Academic Press.

Reches, Z.E. (1978). Analysis of faulting in three-dimensional strain field. *Tectonophysics*, *47*(1-2), 109-129.

Robion, P., Grelaud, S., & de Lamotte, D. F. (2007). Pre-folding magnetic fabrics in fold-and-thrust belts: Why the apparent internal deformation of the sedimentary rocks from the Minervois basin (NE—Pyrenees, France) is so high compared to the Potwar basin (SW—Himalaya, Pakistan)? *Sedimentary Geology*, *196*(1–4), 181–200. https://doi.org/10.1016/j.sedgeo.2006.08.007

Rochette, P., Jackson, M., & Aubourg, C. (1992). Rock magnetism and the interpretation of anisotropy of magnetic susceptibility. *Reviews of Geophysics*, *30*(3), 209–226. https://doi.org/10.1029/92rg00733

Sagnotti, L., Faccenna, C., Funiciello, R., & Mattei, M. (1994). Magnetic fabric and structural setting of Plio–Pleistocene clayey units in an extensional regime: The Tyrrhenian margin of central Italy. *Journal of Structural Geology*, *16*, 1243–1257. https://doi.org/10.1016/0191-8141(94)90067-1

Sagnotti, L., & Speranza, F. (1993). Magnetic fabric analysis of the Plio-Pleistocene clayey units of the Sant'Arcangelo basin, southern Italy. *Physics of the Earth and Planetary Interiors*, *77*(3–4), 165–176. https://doi.org/10.1016/0031-9201(93)90096-R

Scheepers, P. J. J., & Langereis, C. G. (1994). Magnetic fabric of Pleistocene clays from the Tyrrhenian Arc; a magnetic lineation induced in the final stage of the middle Pleistocene compressive event. *Tectonics*, *13*(5), 1190–1200. https://doi.org/10.1029/94tc00221

Scriba, H., & Heller, F. (1978). Measurements of anisotropy of magnetic susceptibility using inductive magnetometers. *Journal of Geophysics*, *44*, 341–352.

Şenel, M. (2002). *1/500.000 scale geological map of Turkey, İzmir, Ankara, Denizli and Konya sheets*. General Directorate of Mineral Research and Exploration (MTA).

Şen, Ş., & Seyitoğlu, G. (2009). Magnetostratigraphy of early-middle Miocene deposits from E-W trending Alasehir and Büyük Menderes grabens in western Turkey, and its tectonic implications. In: D. J. J. van Hinsbergen, M. A. Edwards, & R. Govers (Eds.), *Collision and collapse at the Africa-Arabia-Eurasia subduction zone* (Vol. 311, pp. 321–342). Geological Society of London Special Publication. https://doi.org/10.1144/sp311.13

Shah, S. T., & Özacar, A. A. (2018). Spatial variations of active stress patterns and frequency-magnitude distribution of earthquakes in Western Anatolia, Turkey. Paper presented at the Proceedings of 71st Geological Congress of Turkey, METU.

Şiş, F. S., Kouwenhoven, T. J., Koç, A., & Kaymakcı, N. (2020). Paleobathymetric evolution of the Miocene deposits of the Gömbe sector of the Lycian Foreland and Aksu basins in Antalya, Turkey. *Turkish Journal of Earth Sciences*, *29*(4), 649–663.

Soto, R., Larrasoaña, J. C., Arlegui, L. E., Beamud, E., Oliva-Urcia, B., & Simón, J. L. (2009). Reliability of magnetic fabric of weakly deformed mudrocks as a palaeostress indicator in compressive settings. *Journal of Structural Geology*, *31*(5), 512–522. https://doi.org/10.1016/j.jsg.2009.03.006

Tan, O., Tapirdamaz, M. C., & Yörük, A. (2008). The earthquake catalogues for Turkey. *Turkish Journal of Earth Sciences*, *17*(2), 405–418.

Tarling, D., & Hrouda, F. (Eds.). (1993). *Magnetic anisotropy of rocks* (1st ed.). Springer.

Tatar, O., Gürsoy, H., & Piper, J. D. A. (2002). Differential neotectonic rotations in Anatolia and the Tauride Arc: Palaeomagnetic investigation of the Erenlerdag Volcanic Omplex and Isparta volcanic district, south-central Turkey. Journal of the Geological Society of London, 159, 281–294. https://doi.org/10.1144/0016-764901-035

Taymaz, T., & Price, S. (1992). May 12 Burdur earthquake sequence, SW Turkey: A synthesis of seismological and geological observations. *Geophysical Journal International*, *108*, 589–603. https://doi.org/10.1111/j.1365-246x.1992.tb04638.x

ten Veen, J. H. (2004). Extension of Hellenic forearc shear zones in SW Turkey: The Pliocene–Quaternary deformation of the Eşen Çay Basin. *Journal of Geodynamics*, *37*(2), 181–204. https://doi.org/10.1016/j.jog.2004.02.001

ten Veen, J. H., Boulton, S. J., & Alçiçek, M. C. (2009). From palaeotectonics to neotectonics in the Neotethys realm: The importance of kinematic decoupling and inherited structural grain in SW Anatolia (Turkey). *Tectonophysics*, *473*(1–2), 261–281. https://doi.org/10.1016/j.tecto.2008.09.030

Tosun, L., Avşar, U., Avşar, Ö., Dondurur, D., & Kaymakcı, N. (2021). Active tectonics and kinematics of Fethiye-Göcek Bay, SW Turkey: Insight about the eastern edge of Pliny-Strabo Trenches. *Journal of Structural Geology*, *145*, 104287.

Uzel, B., Langereis, C. G., Kaymakcı, N., Sözbilir, H., Özkaymak, Ç., & Özkaptan, M. (2015). Paleomagnetic evidence for an inverse rotation history of Western Anatolia during the exhumation of Menderes core complex. *Earth and Planetary Science Letters*, *414*, 108–125. https://doi.org/10.1016/j.epsl.2015.01.008

Uzel, B., Sözbilir, H., Özkaymak, Ç., Kaymakcı, N., & Langereis, C. G. (2013). Structural evidence for strike-slip deformation in the Izmir–Balıkesir transfer zone and consequences for late Cenozoic evolution of western Anatolia (Turkey). *Journal of Geodynamics*, *65*, 94–116. https://doi.org/10.1016/j.jog.2012.06.009

van Hinsbergen, D. J. J., Dekkers, M. J., Bozkurt, E., & Koopman, M. (2010). Exhumation with a twist: Paleomagnetic constraints on the evolution of the Menderes metamorphic core complex, western Turkey. *Tectonics*, *29*(3), 1–33. https://doi.org/10.1029/2009TC002596

van Hinsbergen, D. J. J., Kaymakcı, N., Spakman, W., & Torsvik, T. H. (2010). Reconciling the geological history of western Turkey with plate circuits and mantle tomography. *Earth and Planetary Science Letters*, *297*(3), 674–686. https://doi.org/10.1016/j.epsl.2010.07.024

Wasoo, M. H., Özkaptan, M., & Koç, A. (2020). New insights on the Neogene tectonic evolution of the Aksu Basin (SE Turkey) from the anisotropy of magnetic susceptibility (AMS) and paleostress data. *Journal of Structural Geology*, *139*, 104137. https://doi.org/10.1016/j.jsg.2020.104137

Westerweel, J., Uzel, B., Langereis, C. G., Kaymakcı, N., & Sözbilir, H. (2020). Paleomagnetism of the Miocene Soma basin and its structural implications on the central sector of a crustal-scale transfer zone in western Anatolia (Turkey). *Journal of Asian Earth Sciences*, *193*, 104305. https://doi.org/10.1016/j.jseaes.2020.104305

Wortel, M. J. R., & Spakman, W. (2000). Subduction and slab detachment in the Mediterranean-Carpathian region. *Science*, *290*, 1910–1917. https://doi.org/10.1126/science.290.5498.1910